THE ACTION OF THE HYDROCYCLONE

A Thesis Submitted for the Degree of

Doctor of Philosophy

in

The University of London

by

Victor Guillermo Renner

Department of Mining and
Mineral Technology,
Royal School of Mines,
Imperial College,
London, S.W.7.

April, 1976.

ABSTRACT

Measurements of size distributions of particles in specific locations within a hydrocyclone under normal operating conditions were carried out with a new high speed sampling technique especially designed and developed for this purpose.

The size distribution patterns show that classification appears to take place only in a central region of the top section of the hydrocyclone. This suggests the existence of a secondary toroidal vortex in that region.

The behaviour of solids inferred from the size distribution patterns is consistent with previous measurement of relative resident times of particles in a hydrocyclone.

A three-dimensional mathematical model of a cyclone based on the unsteady creeping motion of solid particles in a cyclonic fluid field is presented. Positional size distribution patterns calculated from the model disagree with the patterns obtained experimentally, despite reasonable agreement between calculated and actual classification efficiency curves. The disagreement between model and experiment is thought to be due to absence in the model of secondary recirculation and short circuit flows.

CONTENTS

		Page:
LIST OF FIGURES		iv
LIST OF MOST COMMONLY USED SYMBOLS		vi
CHAPTER 1 -	INTRODUCTION	1
CHAPTER 2 -	UNSTEADY CREEPING MOTION OF A SOLID PARTICLE IN A CYCLONIC FLUID FIELD	6
2.1.	Coordinate System and Characteristic Dimensions	6
2.2.	Analytical Model of a Cyclonic Fluid Flow	6
2.3.	Determination of the Parameters of the Fluid Field	9
2.4.	Equations of Motion of a Solid Particle in the Cyclonic Fluid Model	12
2.5.	Derivation of the Solution of the Equations	15
2.6.	Equilibrium Position and Maximum Particle Size	19
2.7.	Numerical Illustration : Particle Paths	20
2.8.	Classification Efficiency	24
2.9.	Calculation of Positional Size Distributions	24
CHAPTER 3 -	MEASUREMENT OF THE POSITIONAL SIZE DISTRIBUTION WITHIN A HYDROCYCLONE	27
3.1.	Sampling through an Aspirated Nozzle	27
3.2.	The Cyclone System	28
3.3.	The Sampling Probe System	31
3.4.	Test Material and Method of Size Analysis	35
3.5.	Sampling Positions and Test Conditions	36
3.6.	Analysis of the Sampling Conditions	39
3.7.	Results	42
3.8.	Assessment of the Reliability of the Results	42

Page:

CHAPTER 4 - DISCUSSION. COMPARISON OF CYCLONE THEORY WITH EXPERIMENT 48

4.1. Introduction 48

4.2. Effect of Ignoring Recirculation and Short Circuit Flow 48

CHAPTER 5 - BEHAVIOUR OF SOLID PARTICLES WITHIN THE HYDROCYCLONE 53

5.1. Patterns of the Size Distributions within the Hydrocyclone 53

5.2. Qualitative Analyses of Particle Behaviour in the Hydrocyclone. 53

CHAPTER 6 - CONCLUSIONS 59

APPENDICES

1. Approximate Analytical Solution of the Equation $y(\frac{dy}{dx} + 1) = k(\frac{1 - x^4}{x^3})$ 61

2. The Behaviour of the Characteristic Size Fraction in Sampling through an Aspirated Nozzle 64

3. Experimental Procedure 69

4. Tables of Data 74

REFERENCES 97

ACKNOWLEDGEMENTS 98

LIST OF FIGURES

Fig. 1. Streamline pattern of the cyclonic fluid field for a 30° cone. (a) View on a radial plane and (b) view on an axial plane.

Fig. 2. Sketch of the inlet section (Eq. (2.8)).

Fig. 3. Path of a particle of size: (a) 40 μm and (b) 80 μm.

Fig. 4. Envelopes of particle paths for particles of: (a) 79 μm, (b) 61 μm, and (c) 44 μm.

Fig. 5. Sketch of the integrated surface (Eq. (2.39)).

Fig. 6. (a) Diagram of the test cyclone, (b) Detail of the sampling window and membrane plug.

Fig. 7. Layout of the cyclone system.

Fig. 8. (a) Diagram of the sampling probe, (b) Detail of the ends of the sampling tubes.

Fig. 9. Layout of the sampling probe system.

Fig. 10. Spatial distribution of the sampling positions.

Fig. 11. Ratio between the retained size distribution of the feed, overflow and underflow f_i and the cyclone contents f_{cc}.

Fig. 12. Effect of sampling time in the size distributions of samples taken at position D7.

Figs. 13-18. Ratio between the retained size distribution of samples f_s and the cyclone contents f_{cc}.

Fig. 19. Ratio between retained size distributions calculated from the model and the actual cyclone contents at Z = 3.6 and various radial positions.

Fig. 20. Experimental and theoretical classification efficiency curves.

Fig. 21. Sketch of the flow of a vortex pair behind a cylinder in a uniform stream, showing the cyclonic contour.

Fig. 22. Regions of similar size distribution within a hydrocyclone.

Fig. 23. Schematic representation of the flow pattern of particles of: (a) fine size, (b) middle size and (c) coarse size.

Fig. 24. Experimental size distribution ratio as function of velocity ratio.

Fig. 25. Sketch of the arrangement to flush away settled particles from the orifice tube.

LIST OF MOST COMMONLY USED SYMBOLS

A	:	parameter of Eq. (2.14) defined by Eq. (2.15a).
A_s	:	area of sampling orifice.
B	:	parameter of Eq. (2.19) defined by Eq. (2.20a).
C	:	parameter of Eq. (2.19) defined by Eq. (2.20b).
D	:	parameter of Eq. (2.27) defined by Eq. (2.28a).
D_F	:	ratio between the diameter of the circle of area a_f and r_o .
E	:	parameter of Eq. (2.27) defined by Eq. (2.28b).
F	:	parameter of Eq. (2.14) defined by Eq. (2.15b).
H	:	parameter of Eq. (2.14) defined by Eq. (2.15c).
M	:	integration constant defined by Eq. (2.23a).
N	:	integration constant defined by Eq. (2.23b).
P	:	integration constant defined by Eq. (2.30a).
Q	:	integration constant defined by Eq. (2.30b).
IR	:	region defined by (2.8).
R_k	:	value of R at T = Kh.
R*	:	equilibrium radius defined by Eq. (2.33).
R_{Ai} , R_{Bi} R_{Ci} , R_{Di}	:	radial coordinates of the points that bound the ends of the path tube (Fig. 5).
S	:	ratio between the densities of the solid and the fluid.
a_f , A_F	:	area of the inlet section of the cyclone
c	:	concentration of particles.
d_p	:	diameter of particle.
d_{pm}	:	maximum particle size defined by Eq. (2.34).
d_s , D_s	:	side of square of area a_f , A_F.
d_{50}	:	diameter of particle that reports in equal fractions to both overflow and underflow.

d_{70} : diameter of particle which reports 70% to underflow

f : size frequency distribution.

f(r) : function of r.

g, G : gravitational acceleration.

h : integration step.

$\hat{i}$: unit axis vector.

r, R : radial coordinate.

t, T : time.

t_s : sampling time.

u, U : fluid velocity.

v, V : particle velocity.

w_f : amount of particle per unit length defined by Eq. (2.35).

z, Z : axial coordinate.

α : root of characteristic equation of Eq. (2.19) defined by Eq. (2.22a).

α^* : one half of the included angle of the cyclone cone.

β : root of characteristic equation of Eq. (2.19) defined by Eq. (2.22b).

γ : root of characteristic equation of Eq. (2.27) defined by Eq. (2.31a).

δ : root of characteristic equation of Eq. (2.27) defined by Eq. (2.31b).

θ : azimuthal coordinate.

μ : fluid viscosity.

ν : kinetic fluid viscosity.

ρ_p : density of solid particles.

ρ_f : density of fluid.

τ : dummy variable of integration.

General subscripts

c	:	on the cone wall.
i	:	size fraction.
ι	:	at the initial time.
o	:	on entry.
r, R	:	in the radial direction.
z, Z	:	in the axial direction.
θ	:	in the azimuthal direction.

General superscripts

⁻	:	vector.
∧	:	unit vector.

CHAPTER 1

INTRODUCTION

The first patent on hydrocyclones was granted to Bretney [1] in 1891, but their widespread use in the mineral industry has its origin with the Dutch State Mines around 1939. Cyclones are now firmly established in industrial practice for classification and gravity concentration of solids as well as for solid-liquid extraction and liquid-liquid separation.

Since 1939 a considerable volume of work has been devoted to defining design criteria based on the concepts of fluid-and-particle--dynamic actions occurring within a cyclone. In 1965 Bradley published a comprehensive review on the hydrocyclone [2], giving more than 600 related references.

The various empirical formulations that have been proposed are either too vague for practical use or remain restricted to the operational conditions used during measurements and lack more general validity. The number of variables affecting the performance of cyclones is so great that it is unlikely that the problem could be solved by a purely empirical approach.

Equally, the fluid-mechanical actions taking place in a cyclone are so complex that attempted theoretical formulations have failed so far to provide the means for correctly calculating the products to be expected from any given cyclone with a specific feed. Thus, it remains impossible to design a cyclone for a particular purpose or to predict performance with adequate accuracy for a set of given conditions.

In seeking experimental information on cyclone characteristics, most previous investigations have been confined to obtaining

external measurements of, for example, size distributions of the cyclone feed and products, volume splits of feed water and slurry, pressure drop, etc.. Some notable exceptions have been test work by Kelsall [3] and Bradley and Pulling [4] who tried optical internal measurements by means of tracers. Their results, however, were obtained under conditions which do not provide direct evidence of the behaviour of particles under normal operating conditions of cyclones.

It is expected that the classifying action of the hydrocyclone may be fully clarified only on the basis of definite knowledge of the motion experienced by its particulate contents. Measurements are presented in this thesis of the relative size distribution of solids at specific locations within a hydrocyclone. The work was carried out in an attempt to obtain detailed information which might elucidate the classifying action.

Most attempts to explain the classifying action of the hydrocyclone start with the fact that the feed slurry is set in orbiting motion at the periphery of the cyclone while the separated products are discharged through orifices situated on the axis of the cyclone. This implies that there must be a net inward radial flow which would tend to drag the particles in a direction opposed to the centrifugal force induced by the orbital motion. It has been suggested that this determines the size separation because fine or light particles being dominantly dragged by the fluid would move inwards to the overflow discharge, while coarse or heavy particles being subjected to higher centrifugal force would move to the walls, forming the downwards underflow stream.

Mathematical formulations of this interpretation have been based on the assumption, supported by practical and theoretical

estimations [5],[6],[7],[2],[8], that the drag force can be calculated to a first approximation from Stokes' law. Under this condition, Lapple and Shepherd [9] suggested that the equation of radial motion of a solid sphere in a two-dimensional fluid field is:

$$\frac{dv_r}{dt} = \frac{v_\theta^2}{r} - \frac{1}{S}\frac{u_\theta^2}{r} + \frac{18\nu(u_r - v_r)}{Sd_p^2} \qquad (1.1)$$

Most followers of this approach have attempted to assess cyclone performance by considering the positions that particles would attain if they reach dynamic and kinetic equilibrium within the cyclone. In that case, $v_r = 0$, and accepting $v_\theta = u_\theta$, then Eq. (1.1) leads to:

$$d_p^2 = -\frac{18\nu u_r}{(S-1)u_\theta^2}\, r \qquad (1.2)$$

Thus, every particle would be expected to reach equilibrium orbit at a radius directly proportional to the square of its diameter. Various formulae to calculate the size of those particles which are equally divided between the two cyclone products (d_{50} size) have been proposed on the assymption that their orbit is coincident with the zone of zero axial velocity. These formulae differ from each other because of differences in the characteristics ascribed to the cyclone geometry and the fluid field.

In order to include the case of particles reaching the wall before attaining orbits of equilibrium, Rietema [8] assumed dynamic equilibrium only, v_r = constant, for Eq. (1.1). He included the residence time of the particles by further assuming that the axial velocity is also constant.

Owing to the non-dynamic conditions of these theories, they cannot provide a complete description of the motion of the particulate matter and they are therefore not suitable for practical verification, other than of the resulting performance.

A further development of these theories is presented in this thesis in the form of a fully dynamic and three-dimensional model where it is also recognized that, although the fluid motion in a cyclone is basically steady, a travelling particle encounters fluid with continuously varying velocity. The model is based on the equation of the creeping motion of a spherical particle in a variable velocity field suggested by Tchen [10] and later clarified by Corrsin and Lumley [11], Hinze [12] and Soo [13]. This equation is of the following form:

$$\frac{\pi}{6} d_p^3 \rho_p \frac{d\vec{v}}{dt} = 3\pi\mu d_p(\vec{u} - \vec{v}) - \frac{\pi}{6} d_p^3 \text{ grad } p + \frac{\pi}{12} d_p^3 \rho_f \left(\frac{d\vec{u}}{dt} - \frac{d\vec{v}}{dt} \right)$$

$$+ \frac{3}{2} d_p^2 \sqrt{\pi \rho_f \mu} \int_{t_o}^{t} \frac{\frac{d\vec{u}}{dt} - \frac{d\vec{v}}{dt}}{\sqrt{t - \tau}} d\tau + \frac{\pi}{6} d_p^3 \rho_p \vec{g} \qquad (1.3)$$

The term on the left hand side ($\frac{\pi}{6} d_p^3 \rho_p \frac{d\vec{v}}{dt}$) is the force accelerating the particle. The first term on the right hand side ($3\pi\mu d_p(\vec{u} - \vec{v})$) is the steady state drag according to Stokes' law. The second term ($\frac{\pi}{6} d_p^3$ grad p) is the force due to the pressure gradient caused by acceleration of the fluid surrounding the particle. The third term ($\frac{\pi}{12} d_p^3 \rho_f (\frac{d\vec{u}}{dt} - \frac{d\vec{v}}{dt})$) is the force needed to accelerate the apparent mass of the particle relative to the fluid.

The fourth term

$$\left(\frac{3}{2}\, d_p^2 \sqrt{\pi \rho_f \mu} \int_{t_o}^{t} \frac{\frac{d\vec{u}}{dt} - \frac{d\vec{v}}{dt}}{\sqrt{t - \tau}}\, d\tau\right)$$

known as the Basset term, is the viscous resistance due to deviation of the motion from steady state. The last term $(\frac{\pi}{6}\, d_p^3\, \rho_p\, \vec{g})$ is the resultant force of the external potential field, in this case gravity.

The pressure gradient in the second term on the right hand side of Eq. (1.3) is related to the fluid velocity by the Navier-Stokes equation, which, for an incompressible fluid, gives:

$$\text{grad } p = -\rho_f \frac{d\vec{u}}{dt_f} + \mu \text{ rot rot } \vec{u} \qquad (1.4)$$

where $\frac{d\vec{u}}{dt_f}$ is the fluid acceleration following the fluid, which is given by:

$$\frac{d\vec{u}}{dt_f} = \frac{\partial \vec{u}}{\partial t} + \text{grad } \frac{|\vec{u}|^2}{2} + \text{rot } \vec{u} \times \vec{u} \qquad (1.5)$$

CHAPTER 2

UNSTEADY CREEPING MOTION OF A SOLID PARTICLE IN A CYCLONIC FLUID FIELD

2.1. Coordinate System and Characteristic Dimensions

It is convenient to use a cylindrical system of coordinates in which r, Θ, z denote the radial, azimuthal and axial coordinates, respectively. The z-axis corresponds to the cyclone axis with the origin at the vertex of the cyclone cone.

It is convenient also to express all quantities in a dimensionless form. For that purpose, the inlet radius r_o is used as the unit of length, the feed velocity u_o as the unit of velocity and, therefore, $\frac{r_o}{u_o}$ as the unit of time. The dimensionless form of any quantity, obtained by dividing by the corresponding characteristic magnitude, is represented by the same letter, but in capitals.

2.2. Analytical Model of a Cyclonic Fluid Flow

In order to solve the equation of motion of a solid particle that moves in a fluid it is necessary to know the motion of the fluid. Based on Kelsall's measurements of the flow in a cyclone [3], it can be assumed as a first approximation that the velocity field of the fluid comprises a vortical motion around the cyclone axis and a radial inward motion that decreases proportionally to the radial position. Thus, the radial and tangential components of the fluid velocity are respectively:

$$u_r = -\frac{u_{ro}}{r_o}\, r \qquad (2.1)$$

and

$$u_\theta = \frac{u_{\theta o}\, r_o}{r} \qquad (2.2)$$

u_{ro} , $u_{\theta o}$ are respectively the radial and tangential components of the fluid velocity at the initial radius r_o .

The whole flow should satisfy the continuity equation, which in cylindrical coordinates is:

$$\frac{1}{r}\frac{\partial}{\partial r}(ru_r) + \frac{1}{r}\frac{\partial u_\theta}{\partial \theta} + \frac{\partial u_z}{\partial z} = 0;$$

it is found that this equation combined with Eqs. (2.1) and (2.2) leads to:

$$\frac{\partial u_z}{\partial z} = 2\frac{u_{ro}}{r_o} \qquad (2.3)$$

where u_z is the axial component of the fluid velocity.

With rotational symmetry, u_z is function of r and z only, hence integration of Eq. (2.3) gives:

$$u_z = 2\frac{u_{ro}}{r_o} z + f(r) \qquad (2.4)$$

where f(r) is an arbitrary function of r which needs to be determined.

Assuming that the whole flow is limited to the interior of a cone, the component of the fluid velocity normal to the cone surface should be zero. Adding the subscript c to the values of the variables on the cone, this condition is expressed by:

$$u_{zc} \sin \alpha^* - u_{rc} \cos \alpha^* = 0 \qquad (2.5)$$

where α^* is one half of the included angle of the cone.

Evaluating Eq. (2.4) on the cone and introducing Eq. (2.5) gives:

$$u_{rc} \cot \alpha^* = 2 \frac{u_{ro}}{r_o} z_c + f(r_c)$$

which, with $z_c = r_c \cot \alpha^*$ (equation of the cone) and with Eq. (2.1), leads to:

$$f(r_c) = -3 \frac{u_{ro}}{r_o} r_c \cot \alpha^*$$

Therefore, if f(r) on the wall is identical with the above expression, the entire flow bounded by a conical wall will satisfy the continuity equation. One obvious and convenient form of such functions is:

$$f(r) = -3 \frac{u_{ro}}{r_o} r \cot \alpha^*$$

The axial component of the fluid velocity then becomes:

$$u_z = \frac{u_{ro}}{r_o} (2z - 3r \cot \alpha^*) \qquad (2.6)$$

Thus, in dimensionless form, the three components of the fluid velocity (Eqs. (2.1), (2.2) and (2.6)) are:

$$U_R = -U_{RO} R$$

$$U_\theta = \frac{U_{\theta O}}{R} \qquad (2.7a,b,c)$$

$$U_Z = U_{RO}(2Z - 3R \cot \alpha^*)$$

The streamline picture of the flow defined by Eqs. (2.7) is shown in Fig. 1. In brief, the main characteristics of this flow are:

1. The flow rotates around the axis in a vortical fashion.
2. None of the velocity components depends on θ, therefore, the flow is axisymmetrical.
3. The flow is confined within a conical wall.
4. The surface where the axial component of the velocity is zero is conical and divides the flow into two regions : the outer zone between that surface and the conical wall, where the flow is towards the vertex, and the zone inside the surface of zero axial velocity, where the flow is in the opposite direction.
5. The flow is everywhere towards the axis, therefore, there is no recirculation in an axial plane.

All these characteristics, except the last one, agree qualitatively well with the main features of the flow in a cyclone. However, the model does not simulate the secondary circulation observed in the top region of cyclones. So any results obtained from this model must be regarded with this limitation in mind.

2.3. Determination of the Parameters of the Fluid Field

Two conditions are needed to determine the parameters U_{RO} and $U_{\theta O}$ required to specify the flow in the model. Assuming that the inlet section a_f and the feed velocity u_o are known, one of the conditions can be obtained by considering that in the model there is a rhomboid section, as shown in Fig. 2, defined by

$$\cot \alpha^* \leq Z \leq \cot \alpha^* + D_s ; \quad Z \tan \alpha^* - D_s \leq R \leq Z \tan \alpha^* \qquad (2.8)$$

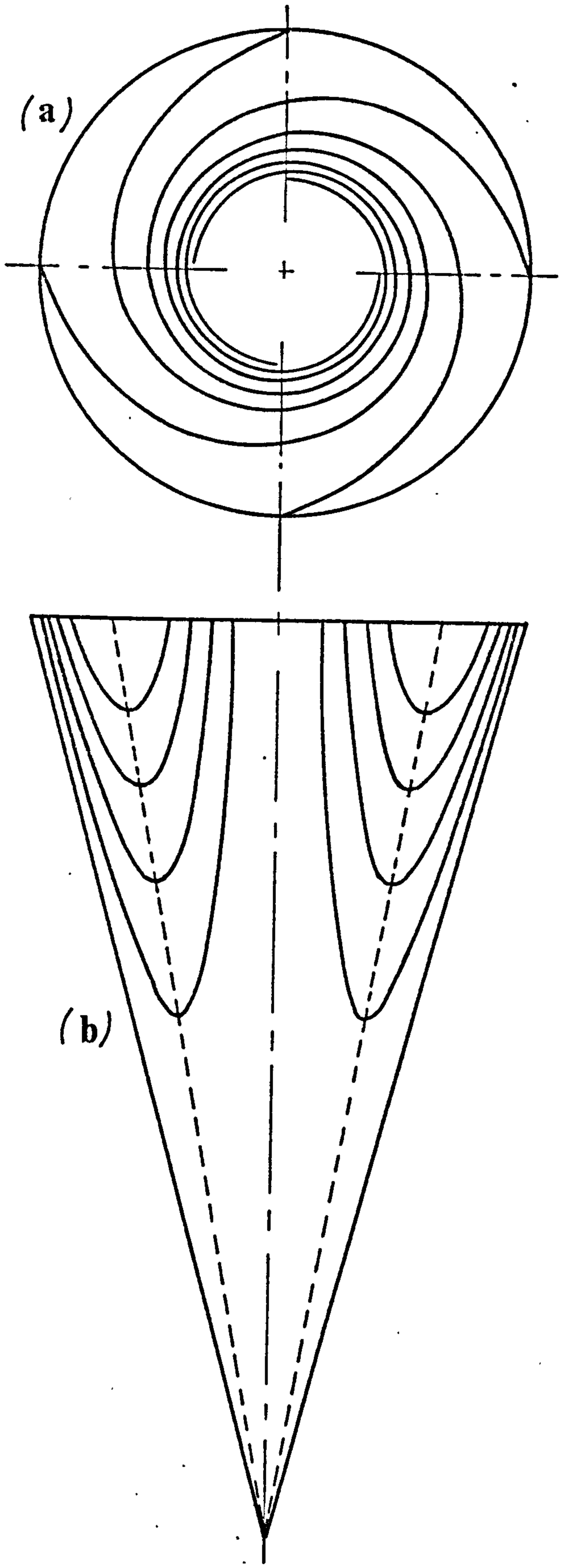

Fig. 1. Streamline pattern of the cyclonic fluid field for a 30° cone. (a) View on a radial plane and (b) view on an axial plane.

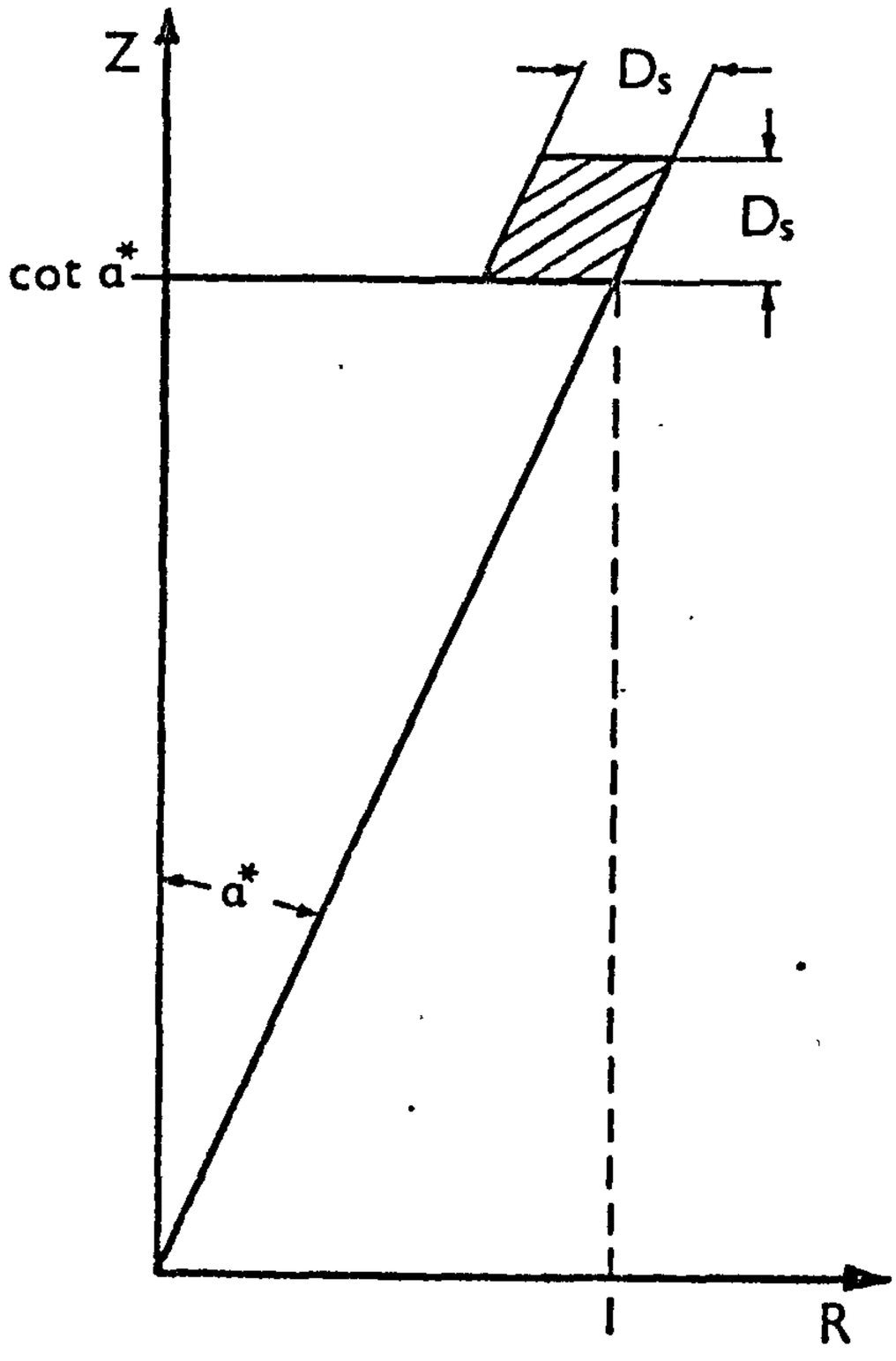

Fig. 2. Sketch of the Inlet Section (Eq. (2.8))

with an area d_s^2 equal to a_f through which there is a flow equal to $u_o \cdot a_f$.

Therefore, in dimensionless form:

$$A_F = \iint_{\mathbb{R}} U_\theta \, dR dZ \qquad (2.9)$$

where $\mathbb{R}$ is the region given by (2.8).

Substituting Eq. (2.7b) into Eq. (2.9), integrating and solving for $U_{\theta O}$, it gives:

$$U_{\theta O} = \frac{A_F}{\cot \alpha^*} \left(X_1 \log \frac{X_1}{X_2} + D_S \log \frac{X_2}{X_3} + \log X_3\right)^{-1} \qquad (2.10a)$$

where:

$$X_1 = 1 + D_S \tan \alpha^* \qquad (2.10b,c,d)$$

$$X_2 = 1 + D_S(\tan \alpha^* - 1)$$

$$X_3 = 1 - D_S$$

The second condition can be obtained by equating the total velocity with the inlet velocity at the entry point R = 1, Z = cot α^*, which gives:

$$U_{RO}^2 + U_{\theta O}^2 + U_{ZO}^2 = 1 \qquad (2.11)$$

with

$$U_{ZO} = - U_{RO} \cot \alpha^* \qquad (2.12)$$

being the value of U_Z at the point considered.

Thus, Eqs. (2.10), (2.11) and (2.13) provide the necessary conditions to specify the parameters of the fluid flow model.

2.4. Equations of Motion of a Solid Particle in the Cyclonic Fluid Model

When the fluid field is known, it is possible to determine the motion of a solid particle that travels in the fluid. Starting from Eq. (1.3) it is assumed that:

1. There are no sudden changes in acceleration so that the Basset term in Eq. (1.3) can be neglected.
2. The displacement between particle paths and fluid streamlines is small, so that the fluid acceleration following the solid

particle, as it appears in the added mass term, can be considered equal to the fluid acceleration following the fluid particles, as it appears in the pressure gradient term (Eq. (1.4)).

3. The pressure gradient is mainly due to the fluid acceleration, so that the viscous contribution can be neglected.

With these simplifications, Eq. (1.3) can be reduced to:

$$\frac{d\vec{v}}{dt} + \frac{36\nu}{dp^2(2S + 1)}\vec{v} = \frac{36\nu}{dp^2(2S + 1)}\vec{u} + \frac{3}{(2S + 1)}\frac{d\vec{u}}{dt} + \frac{2(S - 1)}{(2S+1)}\vec{g} \qquad (2.13)$$

where:

$$S = \frac{\rho_p}{\rho_f}$$

or, alternatively, dividing by $\frac{u_o^2}{r_o}$, the following dimensionless form is obtained:

$$\frac{d\vec{V}}{dT} + A\vec{V} = A\vec{U} + F\frac{d\vec{U}}{dT} + H\vec{G} \qquad (2.14)$$

where:

$$A = \frac{36\nu r_o}{dp^2(2S + 1)u_o}$$

$$F = \frac{3}{2S + 1} \qquad (2.15a,b,c)$$

$$H = \frac{2(S - 1)}{(2S + 1)}$$

If the coordinates of the particles are the cylindrical coordinates R, Θ, Z, and if $\hat{i}_R$, $\hat{i}_\theta$, $\hat{i}_Z$ are the unit vectors in the direction of the axis of the coordinate system, then, from Eqs. (2.7),

$$\vec{U} = -U_{RO} R\hat{i}_R + \frac{U_{\theta O}}{R}\hat{i}_\theta + U_{RO}(2Z - 3R \cot \alpha^*)\hat{i}_Z$$

which, according to Eq. (1.5) gives:

$$\frac{d\vec{U}}{dT} = (U_{RO}^2 R - \frac{U_{\theta O}^2}{R^3})\hat{i}_R + U_{RO}^2(4Z - 3R \cot \alpha^*)\hat{i}_Z$$

In cylindrical coordinates:

$$\vec{V} = \frac{dR}{dT}\hat{i}_R + R\frac{d\Theta}{dT}\hat{i}_\theta + \frac{dZ}{dT}\hat{i}_Z$$

and

$$\frac{d\vec{V}}{dT} = \left[\frac{d^2R}{dT^2} - R(\frac{d\Theta}{dT})^2\right]\hat{i}_R + \left[R\frac{d^2\Theta}{dT^2} + 2\frac{dR}{dT}\frac{d\Theta}{dT}\right]\hat{i}_\theta + \frac{d^2Z}{dT^2}\hat{i}_Z$$

Therefore, Eq. (2.14) can be resolved into its three scalar differential equations, as follows:

$$\frac{d^2R}{dT^2} - R(\frac{d\Theta}{dT})^2 + A\frac{dR}{dT} = -AU_{RO}R + F(U_{RO}^2 R - \frac{U_{\theta O}^2}{R^3})$$

$$R\frac{d^2\Theta}{dT^2} + 2\frac{dR}{dT}\frac{d\Theta}{dT} + AR\frac{d\Theta}{dT} = A\frac{U_{\theta O}}{R} \qquad (2.16a,b,c)$$

$$\frac{d^2Z}{dT^2} + A\frac{dZ}{dT} = AU_{RO}(2Z - 3R \cot \alpha^*) + FU_{RO}^2(4Z - 3R \cot \alpha^*) - HG$$

Using the subscript ι in the quantities evaluated at the initial time $T = 0$, and assuming that at that time the solid particle possesses the same velocity as the fluid in the corresponding entry point, then the initial conditions of Eqs. (2.16) are:

$$\begin{aligned} T &= 0 \\ R &= R_\iota \\ \Theta &= \Theta_\iota \\ Z &= Z_\iota \\ \vec{V} &= \vec{U}_\iota \end{aligned} \qquad (2.17)$$

2.5. Derivation of the Solution of the Equations

Eq. (2.16b), written in the form:

$$\frac{d}{dT}\left(R^2 \frac{d\Theta}{dT}\right) + AR^2 \frac{d\Theta}{dT} = AU_{\theta O} \quad ,$$

can be readily integrated once to give:

$$R^2 \frac{d\Theta}{dT} = ke^{-AT} + U_{\theta O}$$

where k is the integration constant.

The solution with the initial values gives:

$$R_\iota^2 \left(\frac{d\Theta}{dT}\right)_\iota = k + U_{\theta O}$$

but, as $R_\iota \left(\frac{d\Theta}{dT}\right)_\iota = U_{\theta\iota} = \frac{U_{\theta O}}{R_\iota}$, then, $k = 0$.

Hence:

$$R^2 \frac{d\Theta}{dT} = U_{\theta O}$$

and

$$R\left(\frac{d\Theta}{dT}\right)^2 = \frac{U_{\theta O}^2}{R^3} \qquad (2.18)$$

Replacing this result, Eq. (2.16a) becomes:

$$\frac{d^2 R}{dT^2} + A \frac{dR}{dT} + BR = \frac{C}{R^3} \qquad (2.19)$$

where

$$B = - U_{RO}(FU_{RO} - A) \qquad (2.20a,b)$$

$$C = U_{\theta O}^2 (1 - F)$$

Although Eq. (2.19) is nonlinear, it may be treated as if it were linear and solved numerically with the aid of the method of variation of parameters. Indeed, according to that method, the general solution of Eq. (2.19) is:

$$R = Me^{\alpha T} + Ne^{\beta T} + \frac{C}{\alpha - \beta}\left[\int_0^T \frac{e^{\alpha(T-\tau)}}{R^3}\, d\tau - \int_0^T \frac{e^{\beta(T-\tau)}}{R^3}\, d\tau\right] \qquad (2.21)$$

where τ is a dummy variable of integration; M, N are the integration constants;

$$\alpha = \tfrac{1}{2}(\sqrt{A^2 - 4B} - A) \qquad (2.22a)$$

$$\beta = -\tfrac{1}{2}(\sqrt{A^2 - 4B} + A) \qquad (2.22b)$$

Evaluating R and its time derivative from Eq. (2.21) at T = 0 gives:

$$R_i = M + N$$

and

$$-U_{RO}R_i = \alpha M + \beta N$$

hence:

$$M = \frac{R_i(U_{RO} + \beta)}{\beta - \alpha}$$

and (2.23a,b)

$$N = \frac{R_i(U_{RO} + \alpha)}{\alpha - \beta}$$

The difference X between the integrals

$$X_1 = \int_0^T \frac{e^{\alpha(T-\tau)}}{R^3}\, d\tau$$

and

$$X_2 = \int_0^T \frac{e^{\beta(T-\tau)}}{R^3}\, d\tau$$

can be evaluated easily. If h is the integration step, then at T = nh, where n is any integer, the Trapezoid Rule gives:

$$X = X_1 - X_2 = \frac{h}{2}\left[\frac{e^{\alpha nh} - e^{\beta nh}}{R_i^3} + 2\sum_{k=1}^{n-1}\frac{e^{\alpha(n-k)h} - e^{\beta(n-k)h}}{R_k^3}\right] \qquad (2.24)$$

where R_k is the value of R at T = kh.

Thus, X becomes independent of R at T = nh and, therefore, starting the calculation with the given initial values, X can be evaluated directly with the recurrence formulae:

$$X_{j+1} = \frac{h}{2}\left[\left(X_j' + \frac{2}{R_j^3}\right)e^{\alpha h} - \left(X_j'' + \frac{2}{R_j^3}\right)e^{\beta h}\right] \qquad (2.25)$$

where:

$$X_j' = \frac{e^{\alpha jh}}{R_i^3} + 2\sum_{k=1}^{j-1}\frac{e^{\alpha h(j-k)}}{R_k^3}$$

$$X_j'' = \frac{e^{\beta jh}}{R_i^3} + 2\sum_{k=1}^{j-1}\frac{e^{\beta h(j-k)}}{R_k^3} \qquad (2.26a,b)$$

An alternative method to solve Eq. (2.19) is presented in Appendix 1.

The third equation of motion, Eq. (2.16c), is of the form:

$$\frac{d^2Z}{dT^2} + A\frac{dZ}{dT} - DZ = -ER - HG \qquad (2.27)$$

where

$$D = 2U_{RO}(A + 2FU_{RO})$$

and (2.28a,b)

$$E = 3U_{RO}(A + FU_{RO})\cot\alpha^*$$

then, since R, as a function of time, is already determined by the preceding procedure, the right hand side of Eq. (2.27) can be calculated readily as a function of time and, in this case, the method of variation of parameters can give the general solution

directly, as follows:

$$Z = Pe^{\gamma T} + Qe^{\delta T} + \frac{1}{\delta - \gamma} \int_0^T (ER + HG)(e^{\gamma(T-\tau)} - e^{\delta(T-\tau)})d\tau \qquad (2.29)$$

where P, Q are the integration constants, which with the given initial conditions are:

$$P = \frac{U_{RO}(2 - 3R_i) - \delta}{\gamma - \delta} \cot \alpha^* \qquad (2.30a,b)$$

$$Q = \frac{U_{RO}(2 - 3R_i) - \gamma}{\delta - \gamma} \cot \alpha^* \quad ; \qquad (2.31a,b)$$

and

$$\gamma = \tfrac{1}{2}(\sqrt{A^2 + 4D} - A)$$

$$\delta = -\tfrac{1}{2}(\sqrt{A^2 + 4D} + A)$$

Finally, the integral of Eq. (2.18) gives:

$$\Theta = U_{\theta O} \int_0^T \frac{dT}{R^2} \qquad (2.32)$$

There remains only the evaluation of the integrals in Eqs. (2.29) and (2.32), but since R is already determined numerically as a function of time, the Trapezoid Rule provides again a convenient method for these two integrations.

2.6. Equilibrium Position and Maximum Particle Size

A particle reaches dynamic and kinetic equilibrium in the radial direction when $\frac{dR}{dT} = 0$; then the equilibrium radius R^*,

according to Eq. (2.19) is:

$$R^* = \left(\frac{C}{B}\right)^{\frac{1}{4}}$$

Replacing C and B from Eqs. (2.20) and A and F from Eqs. (2.15), R^* is expressed by:

$$R^* = \left(\frac{2u_{\theta o}^2 (S - 1) d_p^2}{36 \nu r_o u_{ro} - 3u_{ro}^2 d_p^2} \right)^{\frac{1}{4}} \qquad (2.33)$$

If R^* is equal to or greater than one, the particle stays at the wall or moves there immediately. Thus, the size d_{pm} of the coarsest particles that can move inside the cyclone, obtained by setting $R^* = 1$, is:

$$d_{pm}^2 = \frac{36 \nu r_o u_{ro}}{2u_{\theta o}^2 (S - 1) + 3u_{ro}^2} \qquad (2.34)$$

2.7. Numerical Illustration : Particle Paths

In order to calculate the solution of the equations of motion of a particle in the model it is first necessary to specify the following parameters : the particle size d_p , the feed velocity u_o , the inlet section a_f , the inlet cyclone radius r_o , the cone angle $2\alpha^*$, the density ratio S, the kinetic viscosity of the fluid ν and the initial radial position of the particle R_i .

All the calculations needed to obtain particle paths (section (2.5)) were linked in one computer program. The same integration step was used in all integrations carried out using Trapezoid Rule and a sequence of solutions was computed by successively halving the trapezoid width until convergence. The solution of Eq. (2.19)

agrees perfectly with the solution obtained by the method of Appendix 1 within the numerical approximations used.

Fig. 3 shows the calculated paths for particles of 40 and 80 μm that start at $R_i = 0.85$ with $u_o = 200$ cm S^{-1}, $a_f = 3.14$ cm^2, $r_o = 7.5$ cm, $\alpha^* = 15°$, $S = 2.65$ and $\nu = 0.01$ $cm^2 S^{-1}$ corresponding to the conditions of the tests described in Chapter 3.

Similarly, Fig. 4 shows projections of calculated surfaces that envelope the path of particles of 44, 61 and 79 μm, for various initial positions under the same conditions. These positions are chosen so that they split the incoming feed into sections containing equal proportions of particles. They are calculated on two assumptions : Firstly, that the motion of all the particles starts at $Z = \cot \alpha^*$ on the interval $1 - D_F \leq R \leq 1$, where D_F is the ratio between the diameter of the circle of area a_f and r_o, and, secondly, that in the interval the particles have a circular continuous distribution, the amount of particles per unit of length w_f being given by:

$$w_f = \sqrt{1 - (x - 1)^2} \qquad (2.35)$$

where x is the coordinate along the interval such that $x = 0$ when $R = 1 - D_F$ and $x = 2$ when $R = 1$. Thus, splitting the feed into n equal fractions, the coordinates x_k of the kth. dividing point satisfies:

$$\frac{k}{n} = \frac{\int_0^{x_k} w_f \, dx}{\int_0^{2} w_f \, dx}$$

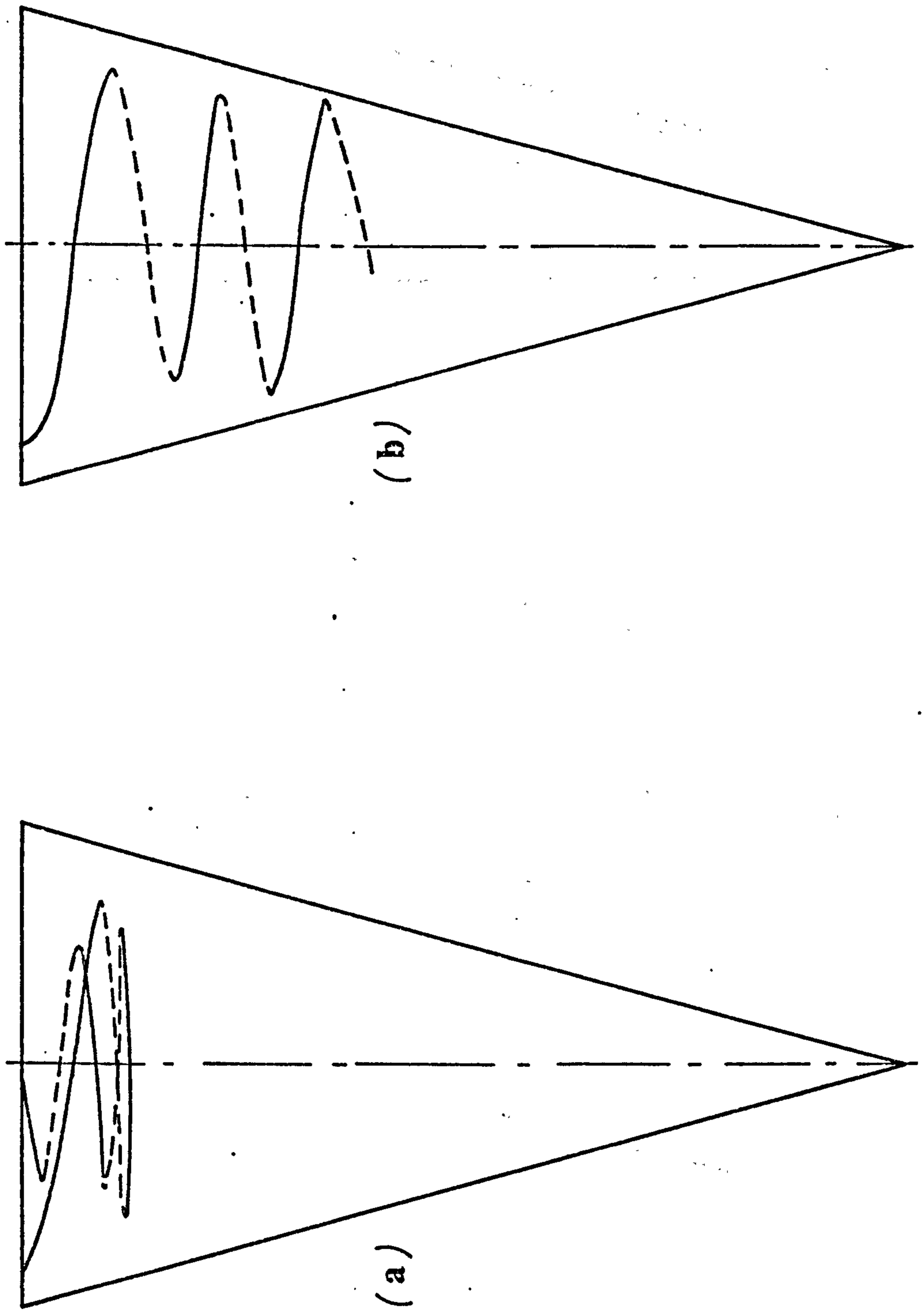

Fig. 3. Path of a particle of size: (a) 40 μm and (b) 80 μm.

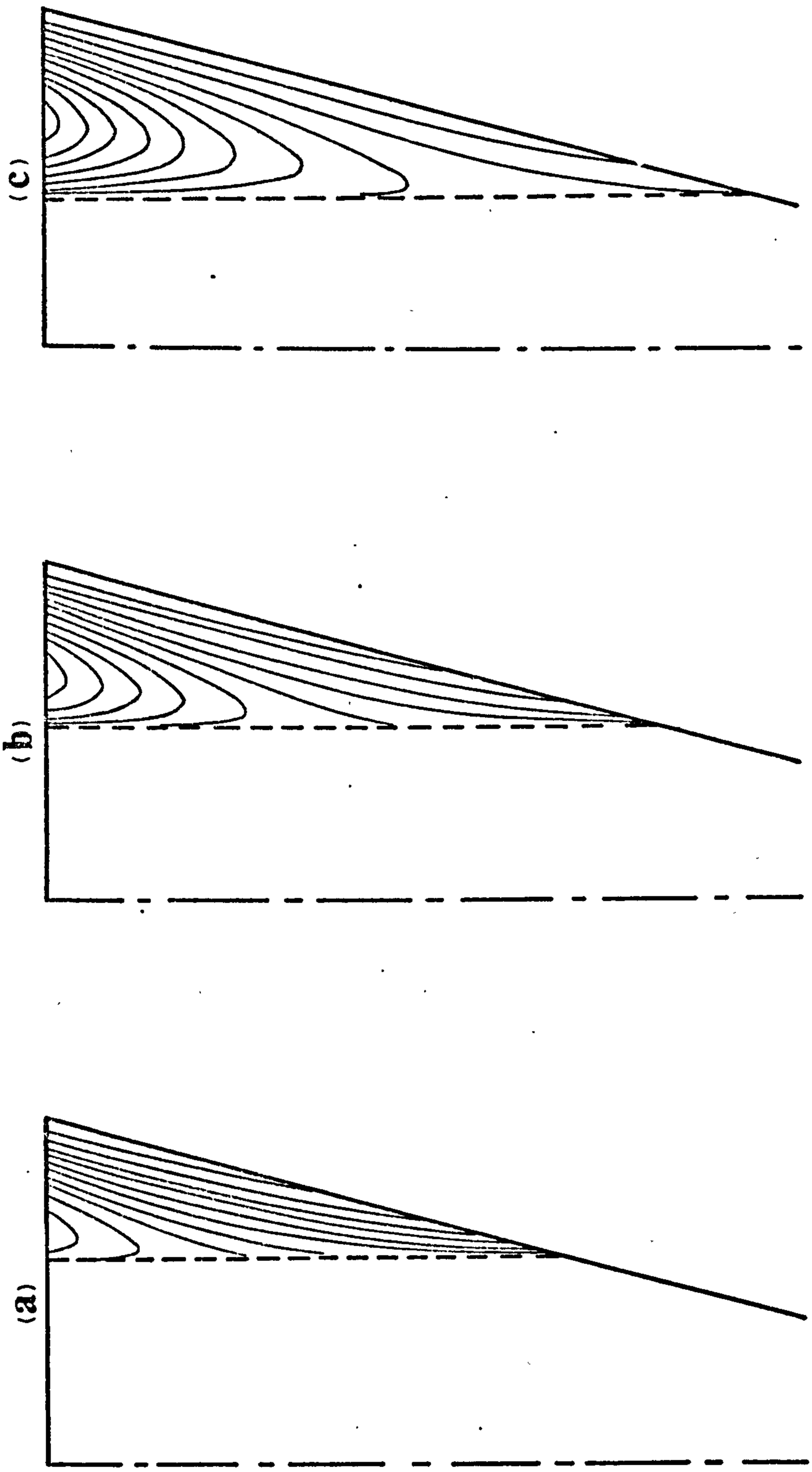

Fig. 4. Envelopes of particle paths for particles of:
(a) 79 μm, (b) 61 μm and (c) 44 μm.

which, after integration gives:

$$\frac{k}{n} = \frac{1}{\pi}\left[(x_k - 1)\sqrt{x_k(2 - x_k)} + \text{arc sin}(x_k - 1) + \frac{\pi}{2}\right] \quad (2.36)$$

2.8. Classification Efficiency

The classification efficiency, defined by the proportion of feed solids in each size fraction going to the underflow, can be obtained from the model by the proportion of feed solids which do not reverse their axial motion within the cyclone body.

Computed values obtained with the initial positions derived from Eq. (2.36) are presented later (Chapter 4) for comparison with experimental data.

2.9. Calculation of Positional Size Distributions

Because of the large number of particles in every size fraction, the condition of conservation of material can be expressed by the equation of continuity of a continuous medium. For steady state and over any volume $\forall$, this is expressed by:

$$\int_{\forall} \text{div}(c_i \vec{v}_i)\, d\forall = 0 \quad (2.37)$$

where c_i and $\vec{v}_i$ are the absolute concentration and the velocity of particles of size i, respectively.

Application of the divergence theorem transforms Eq. (2.37) in:

$$\oint_{\Lambda} c_i \vec{v}_i \cdot \hat{n}\, d\Lambda = 0 \quad (2.38)$$

where Λ is the closed surface that bounds the volume $\forall$ and $\hat{n}$ is the unit outward vector normal to the surface.

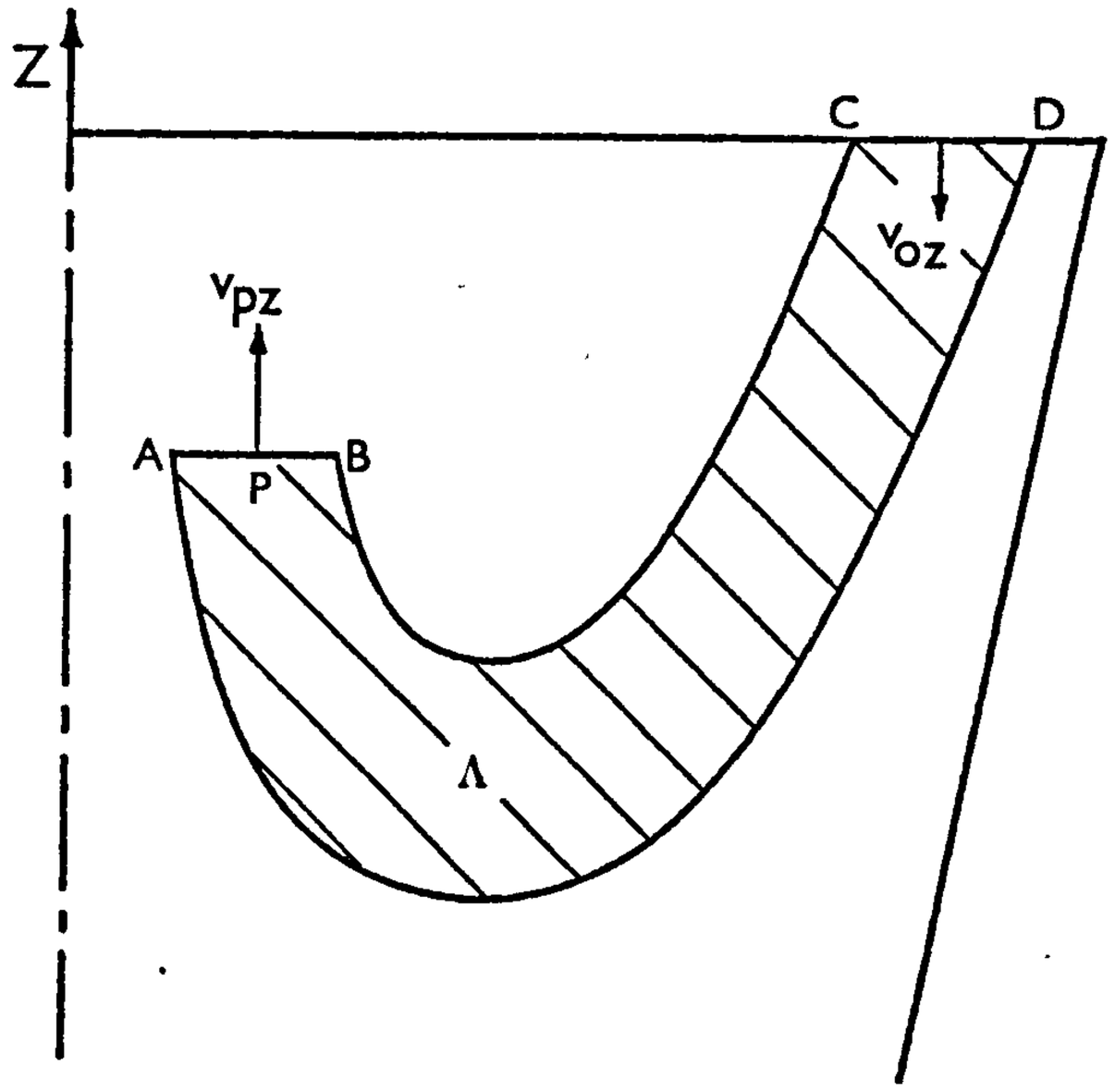

Fig. 5 Sketch of the Integrated Surface (Eq. (2.39))

Since the velocity field $\vec{v}_i$ of the solid particles can be readily obtained from the trajectories resulting from the model, the concentration c_i at any point can be calculated when the concentrations at entry into the cyclone are given. In particular, if the surface Λ is chosen so that it coincides with a path tube with one end containing the point P where the concentration is to be calculated, as sketched in Fig. 5, the other end being at the entry level, then integration of Eq. (2.38) gives:

$$c_{pi}\, v_{pzi}\, (R_{Ai}^2 - R_{Bi}^2) = c_{oi}\, v_{ozi}\, (R_{Ci}^2 - R_{Di}^2) \qquad (2.39)$$

where:

c_{pi} is the average concentration of particles of size i over the circumference that contains P on the radial plane.

c_{oi} is the concentration of particles of size i on entry.

R_{Ai} , R_{Bi} and R_{Ci} , R_{Di} are the radial coordinates of the points that bound the ends of the surface at the level of P and at the entry level, respectively.

v_{pzi} , v_{ozi} are the mean axial components of the velocity of particles of size i over the ends of the surface at the level P and entry, respectively.

The usual data for cyclone operation are the relative rates of entrance f_{oi} of the various size fractions, which with the present notation are expressed by:

$$f_{oi} = \frac{c_{oi}\, v_{ozi}}{\sum_i c_{oi}\, v_{ozi}} \qquad (2.40)$$

By combining Eq. (2.39) with Eq. (2.40), the size frequency distribution of the particles at the point P, given by:

$$f_{pi} = \frac{c_{pi}}{\sum_i c_{pi}} \qquad (2.41)$$

becomes:

$$f_{pi} = \frac{\Omega_i\, v_{pzi}^{-1}\, f_{oi}}{\sum_i \Omega_i\, v_{pzi}^{-1}\, f_{oi}} \qquad (2.42)$$

where:

$$\Omega_i = \frac{R_{Ci}^2 - R_{Di}^2}{R_{Ai}^2 - R_{Bi}^2}$$

Results of these calculations are presented later in Chapter 4.

CHAPTER 3

MEASUREMENT OF THE POSITIONAL SIZE DISTRIBUTION WITHIN A HYDROCYCLONE

A high speed sampling technique was developed for inserting a sampling probe into chosen positions within a hydrocyclone in order to determine the relative concentration distribution of particles of various sizes.

Attainment of this objective was initially attempted by using a radiofrequency detection technique which measures the influence of magnetic particles on the "Q" factor of a coil placed against the cyclone wall in different positions. This technique was abandoned because its sensitivity was insufficient for detecting particles which were not close to the cyclone wall.

3.1. Sampling through an Aspirated Nozzle

A spot sample may be collected by opening a small orifice in a probe inserted in a moving suspension. The quantity of particles of a given size thus collected is the product of the absolute concentration c_i of the particles of that size at the sampling point, the component v_{xi} of the velocity of those particles in the direction normal to the sampling orifice, the area A_s of the orifice, and the sampling time t_s. Therefore, the size frequency distribution f_{xi} of the solids in the sample is:

$$f_{xi} = \frac{c_i v_{xi} A_s t_s}{\sum_i c_i v_{xi} A_s t_s} = \frac{c_i v_{xi}}{\sum_i c_i v_{xi}} \qquad (3.1)$$

which is also referred to as the "transport concentration" of the particles of size i in the direction x.

If a true transport concentration is to be obtained by means of an aspirated nozzle, the insertion of the sampling device into the cyclone and the withdrawal of the sample must cause the minimum disturbance to the flow pattern. This may be achieved under two conditions : Firstly, the time between the insertion of the sampling probe and the end of the sampling action must be shorter than the time beyond which the new flow configuration can start to affect the solid distribution at the sampling point. Secondly, either the velocity at which the sample is withdrawn must be the same as that of the stream at the sampling point or the sampling time must be so small that the disturbance caused by the sampling action has no time to develop.

Alternatively, it was thought that if the second condition could nct be met in practice, some information about the true size distribution at any point within the cyclone could be obtained by taking more than one sample at the same point using different rates of sampliry. This was based on an analytical conclusion, supported by preliminary tests in a pipe, on sampling through an aspirated nozzle. It was shown that there is a characteristic size fraction whose relative proportion in the sample is independent of the sampling velocity and, therefore, is equal to the true proportion of that size fraction in the stream. The analysis and the experimental verification are reported in Appendix 2.

3.2. The Cyclone System

A cyclone, whose dimensions are given in Fig. 6a, was specially constructed for this project. The cylindrical and conical sections were made in one piece of moulded resin. The roof is level, adjusted to be perfectly in line with the top of the inlet pipe and

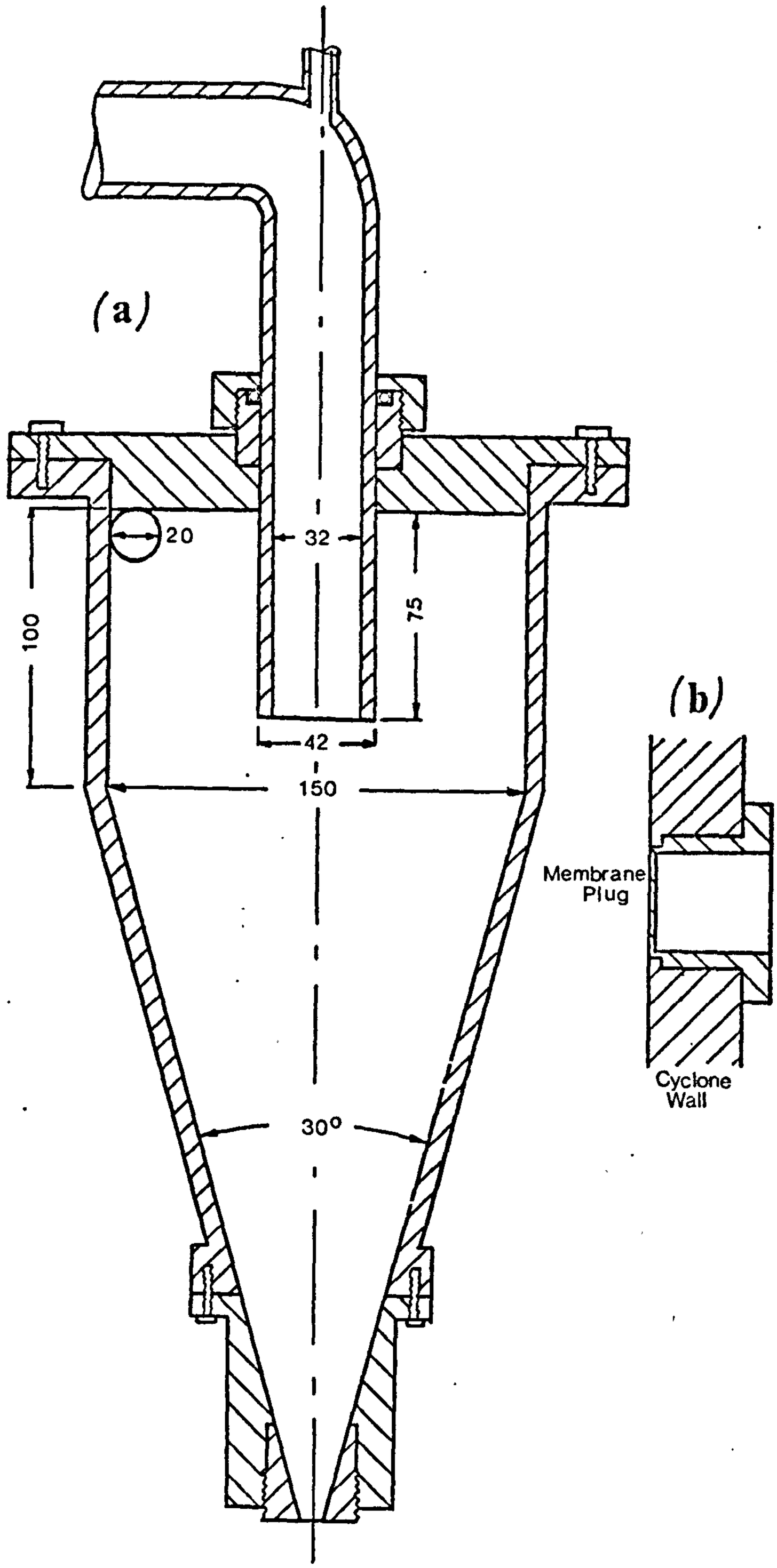

Fig. 6. (a) Diagram of the test cyclone.
(b) Detail of the sampling window and membrane plug.

(Dimensions in mm)

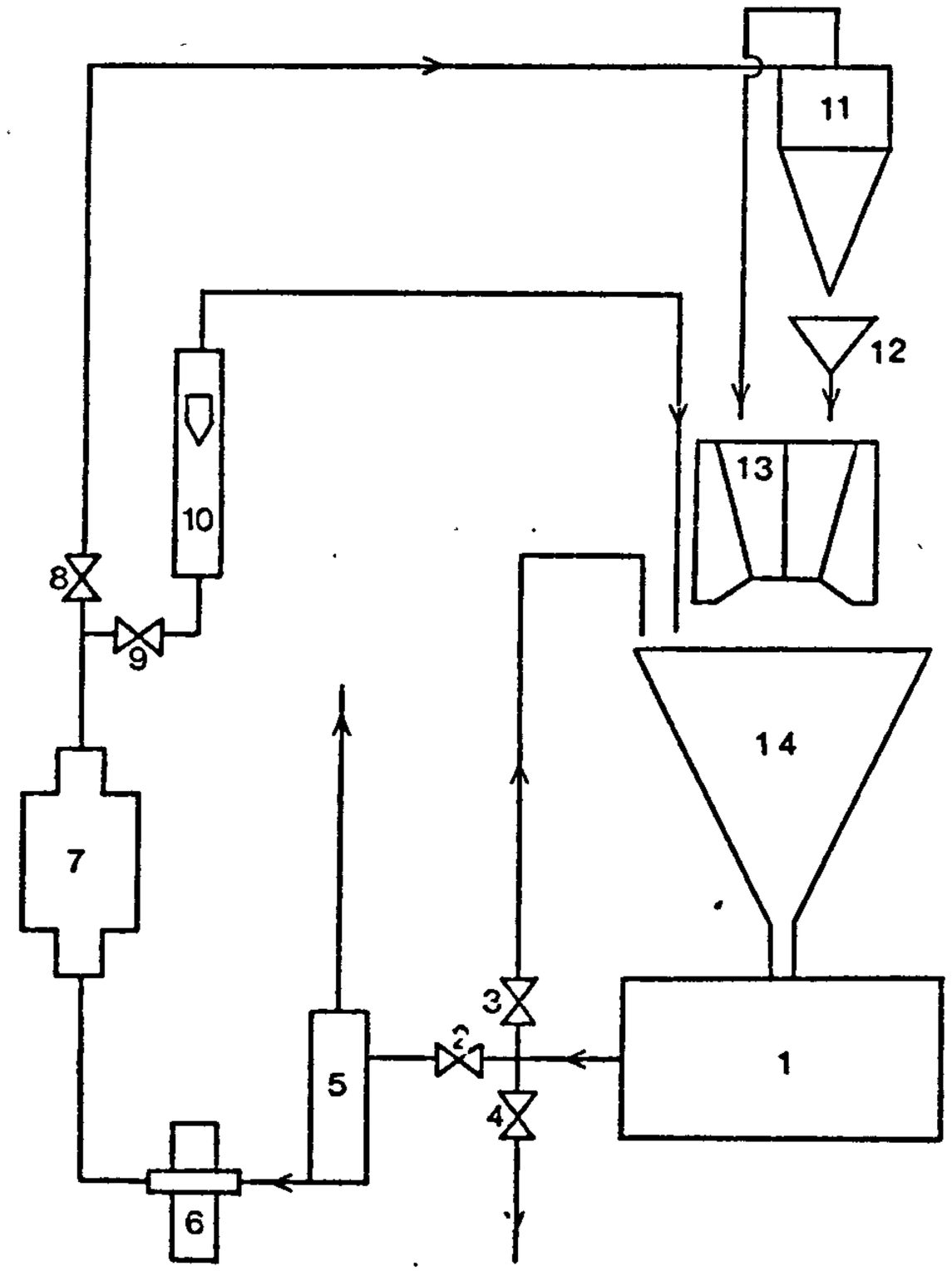

1. Pump:
2. Main flow valve:
3. By-pass valve:
4. Drain valve:
5. De-aerator:
6. Density gauge:
7. Electromagnetic flow-meter:
8. Main flow valve:
9. By-pass valve:
10. Rotameter:
11. Cyclone:
12. Funnel:
13. Twin sampler:
14. Sump:

Fig. 7. Layout of the cyclone system.

is bolted to the main body. The diameter of the underflow outlet can be varied by changing the apex unit screwed to the bottom of the conical section. The overflow pipe is vented to atmosphere to avoid syphoning action.

For the insertion of a sampling probe in a chosen position during a test, a window was cut in the cyclone body and plugged with a prefabricated thin resin membrane (Fig. 6b). When the probe was moved to a different site, the sampling window was obliterated by re-moulding.

A diagram of the cyclone system is shown in Fig. 7. The cyclone was in closed circuit with a type D6, two inch Mono pump. The flow rate and the density of the slurry were continuously monitored with a Kent Veriflux electromagnetic flow-meter and a Baldwin Atomette gamma-ray transmission gauge respectively. The slurry, before being monitored, passed through a centrifugal de-airator. The rotameter, in a by-pass branch, was installed to facilitate checking of the electromagnetic flow-meter. The cyclone overflow and underflow were returned to the pump via a twin sampler capable of taking simultaneous samples of the two products. A by-pass to the sump was used to control the flow-rate to the cyclone and it was discharged through a perforated tube at high velocities to produce good mixing.

3.3. The Sampling Probe System

A new and specially designed probe, shown schematically in Fig. 8a, was used to sample the contents of the cyclone. It consists of two coaxial tubes (A) whose ends, shown in detail and with dimensions in Fig. 8b, penetrate the cyclone by breaking the membrane in the wall window. The clearance between the tubes is

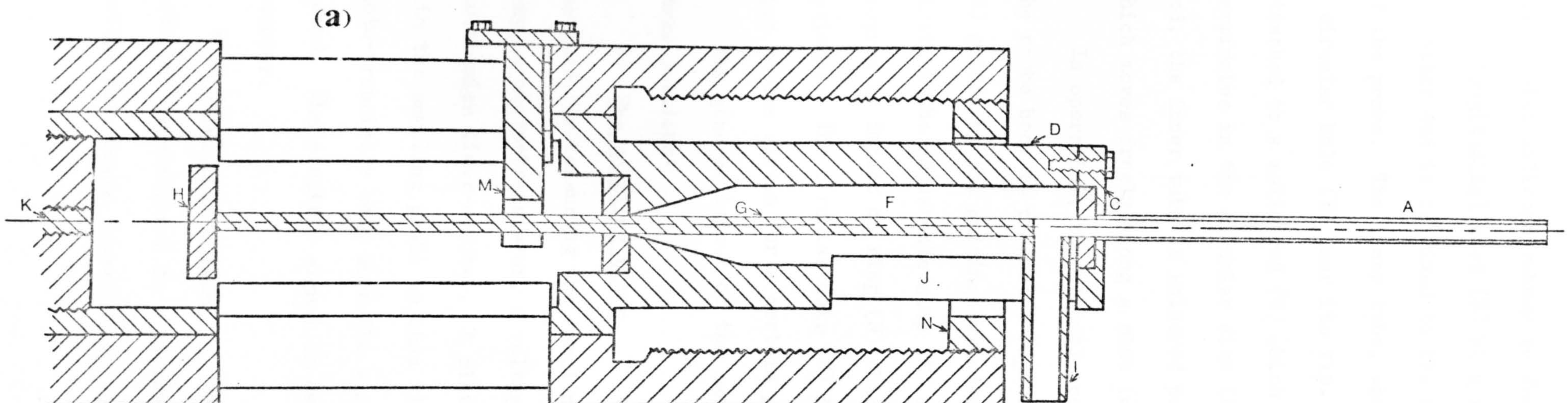

A coaxial tubes:
B slot:
C flange:
D probe body:
E circular orifice:
F chamber:
G rod:
H circular disc:
I perpendicular tube:
J chamber slot:
K pneumatic piston:
L guiding cylinder:
M adjustable stopper:
N screwed ring:

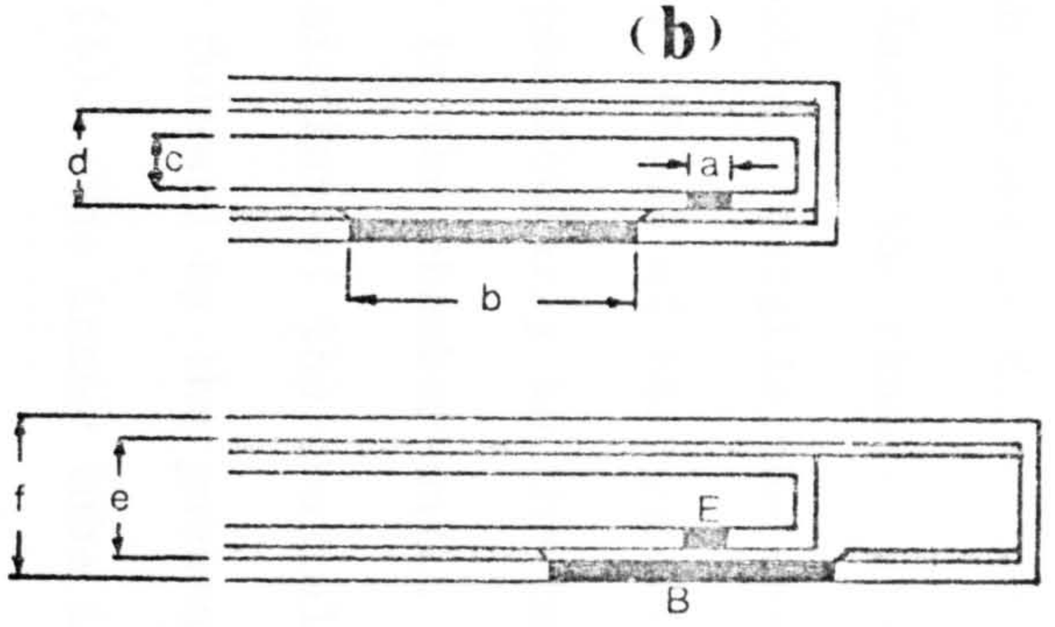

Fig. 8. (a) Diagram of the sampling probe.
(b) Detail of the ends of the sampling tubes. (a = 3.0 mm; b = 22.0 mm; c = 4.2 mm; d = 5.1 mm; e = 6.3 mm; f = 7.9 mm).

filled with silicone rubber to form a sliding seal. The outer tube has a longitudinal slot (B) at a short distance from its tip. At the other end it is fixed to the flange (C) bolted to the body (D) of the probe. The inner tube, which slides in the outer tube, has a circular hole (E) near its tip. Inside the chamber (F) it is attached to a solid rod (G) which extends outside the chamber and terminates in the circular disc (H). Ahead of the junction with the rod, the inner tube is soldered perpendicularly to the tube (I) which moves freely along a slot (J) in the chamber wall.

In operation, the assembly consisting of the coaxial tubes and the probe body is projected rapidly forward by the pneumatic piston (K) guided by the guiding cylinder (L). The inner tube is halted first by the adjustable stop (M) and the rest of the probe is stopped by impact on ring (N) which is screwed to the guiding cylinder. The circular hole (E) in the inner tube thus remains open to the stream for a certain period of time in a fixed position.

The general layout of the sampling system (Fig. 9) comprises three sections:

i) <u>The sampling timer.</u> An electro-optical device was designed for measuring the sampling time. It consists of a microscope lamp, a photo-transistor, a voltage amplifier and a TC6 Advance Electronics timer-counter. A plate with two parallel slots moves with the sampling probe so that light from the lamp can reach the photo-transistor only when the sampling orifice is being opened or closed. The electric signal is amplified to trigger the timer--counter.

ii) <u>Sample extraction.</u> The inner tube of the sampling probe can be connected to a vacuum line via tube (I) (Fig. 8a). Suction for sample removal supplied by an oil vacuum pump is

1. Sampling probe:
2. Microscope lamp:
3. Phototransistor:
4. Voltage amplifier:
5. Timer counter:
6. Vacuum line:
7. Bottle trap:
8. Manometer:
9. Valve to atmosphere:
10. Vacuum pump:
11. Pneumatic piston:
12. Manual valve:
13. Lubricator:
14. Pressure gauge:
15. Filter:
16. Control valve:
17. Compressed air supply:

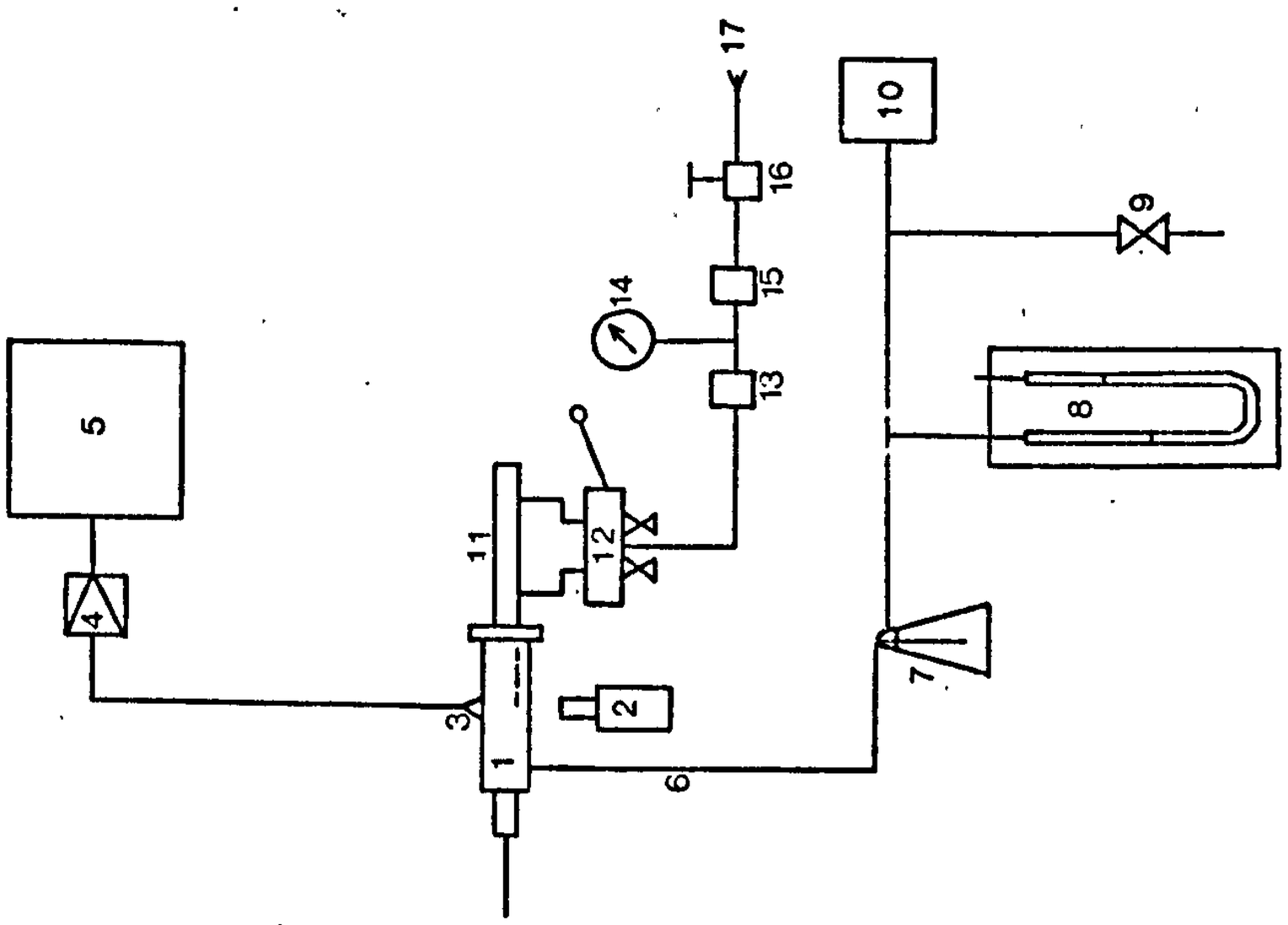

Fig. 9. Layout of the sampling probe system.

measured by a mercury manometer. After each test, all solid particles of the sample are washed out of the probe into a bottle trap without the probe having to be opened.

iii) Probe piston actuator. The thrust to actuate the probe is provided by a pneumatic piston operated with compressed air from the laboratory supply, or from a compressed air cylinder if the pressure required exceeds 100 psi. The line contains a control valve, a filter, a gauge to measure the pressure and a lubricator. A two-way manual valve actuates the piston whose speed can be regulated by adjusting two throttle valves on the delivery side.

3.4. Test Material and Method of Size Analysis

Quartz sand of approximately constant size distribution was used in all tests. The quantity of sand consumed in each test was about 7 kg. Because the size distribution of the charge was altered by each test, it was necessary to prepare large amounts of equal batches of sand. These were obtained by riffling about 1 ton of feed material that had been produced by sieving sand supplied by British Industrial Sands Ltd. designated as grade "HH" Redhill. The raw sand was sieved on 150 mesh (BS) screens, using three 20" Russell shakers in series. The size distribution obtained was about 5 percent coarser than 150 mesh (106 μm) due to imperfections in the screens used.

All size analyses were carried out with a "Model ZB Industrial" Coulter counter using either a 400 μm or a 280 μm orifice tube. The procedure for the preparation and sizing of samples is described separately in Appendix 3B.

3.5. Sampling Positions and Test Conditions

The samples were taken along lines perpendicular to the walls of the cyclone and aligned in an axial plane at 60° from the inlet in the direction of the feed. As shown in Fig. 10, the sampling positions are designated by letters, referring to the line upon which they lie, and by numbers, referring to their relative order in the line. The coordinates of these positions are included in the tables of Appendix 4.

The operating procedure is described in Appendix 3A. In all tests the cyclone was operated under approximately identical conditions, chosen principally to produce similar solid flow rates in the cyclone products and a free spray discharge through the apex outlet. The operating data and results are tabulated in full in Table 1. An assessment of the reliability of those figures is given at the end of this chapter.

The temperature of the slurry was not controlled, but was measured before sampling during every test. Temperatures fluctuated between 24°C and 30°C and are tabulated with the results of the corresponding tests in Appendix 4.

The size distributions of the cyclone feed, overflow and underflow are presented graphically in Fig. 11 as a ratio of the corresponding size frequency distribution and the size frequency distribution of the whole cyclone contents. The recovery of solids in the underflow as a function of particle size, or classification efficiency, is plotted in Fig. 20 (Chapter 4) together with the values predicted from the theoretical model for corresponding conditions.

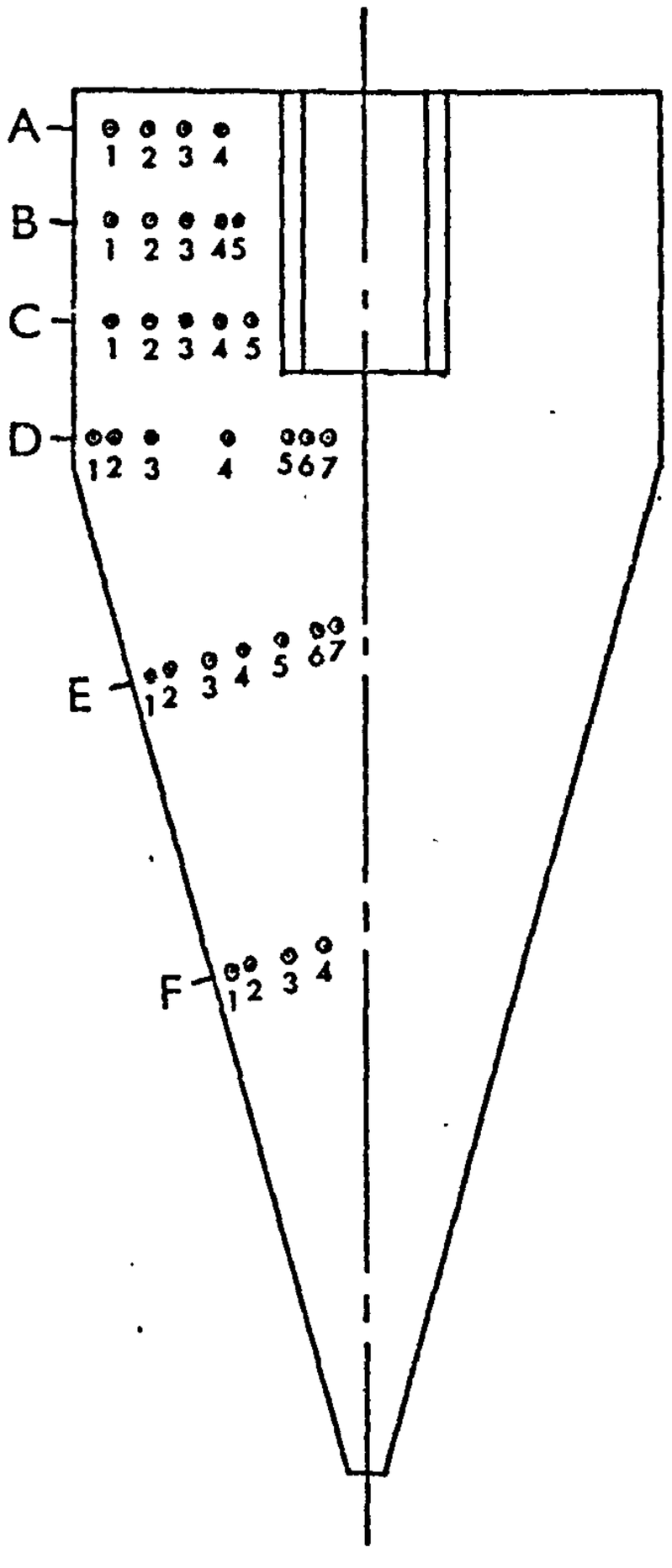

Fig. 10. Spatial distribution of the sampling positions.

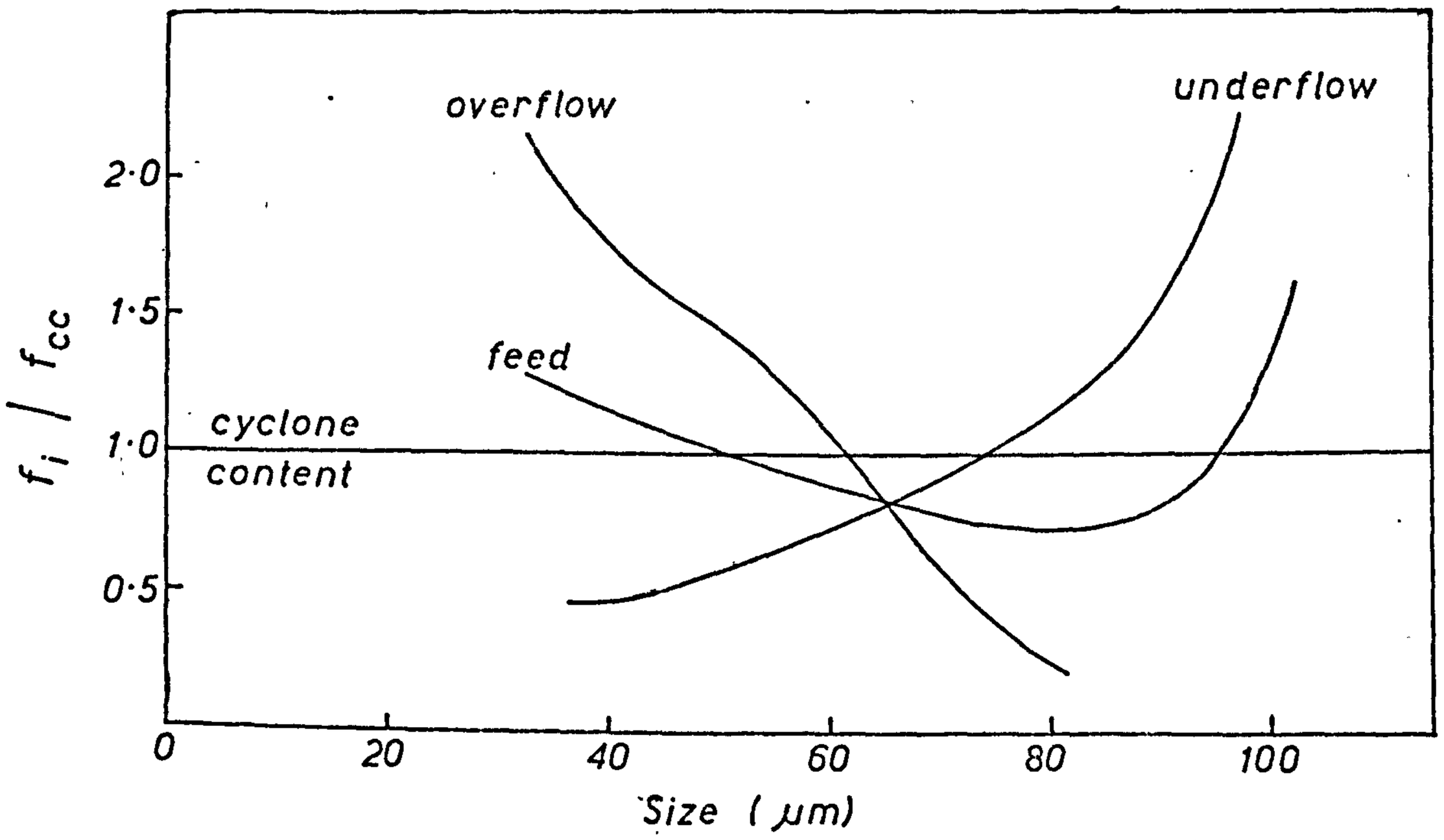

Fig. 11. Ratio between the retained size distribution of the feed, overflow and underflow f_i and the cyclone contents f_{cc}.

Table 1. Cyclone Operating Data*

	$\bar{x}$	k	s
Feed rate, $cm^3 s^{-1}$	620	-	-
Underflow diameter, cm	1.0	-	-
Solids in feed, weight %	21.5	0.2	1.0
Solids in underflow, weight %	59.4	0.2	0.8
Solids in overflow, weight %	13.0	0.2	0.9
Slurry to underflow, volume %	18.3	0.2	1.0
Solids to underflow, weight %	50.6	0.6	2.5

Size Analyses, Cumulative Weight %**

	Feed		Underflow		Overflow		Cyclone Content
Size (μm)	$\bar{x}$	s	$\bar{x}$	s	$\bar{x}$	s	$\bar{x}$
20	4.6	0.9	3.0	0.7	6.5	1.9	1.9
30	11.5	1.9	6.3	1.4	17.1	4.0	6.0
40	20.7	2.0	9.9	1.7	32.5	4.1	13.6
50	33.8	1.2	16.0	1.8	53.1	3.2	25.9
60	50.0	1.1	26.7	1.6	75.3	2.7	42.4
70	65.7	1.3	41.8	1.2	91.3	1.8	61.0
80	78.1	1.0	59.3	1.0	98.2	0.9	78.1
90	87.3	0.6	75.6	1.1	-	-	90.4
100	93.4	0.5	87.2	1.2	-	-	96.6
110	96.4	0.6	93.0	1.2	-	-	98.0

* $\bar{x}$: mean value; $\bar{x} \pm k$: 95% confidence interval for the mean; s : standard deviation.

** 95% confidence interval for the mean is $\bar{x} \pm 0.86$ s.

3.6. Analysis of the Sampling Conditions

It was estimated that the speed at which the sampling probe was introduced into the cyclone was a few hundred times greater than the radial component of the velocity in the hydrocyclone. On the other hand, the flow in a cyclone is predominantly orbital, therefore, the time for the disturbance to travel back to its origin should be no less than the period of one revolution. Therefore, whether a sample is affected by the disturbance depends primarily on the sampling time during which the inner tube of the probe remains stationary.

In all sampling tests the sampling orifice faced in the azimuthal direction of the cyclone. According to Eq. (3.1), the size frequency distribution of a true sample taken in that direction is given by:

$$f_{\theta i} = \frac{c_i v_{\theta i}}{\sum_i c_i v_{\theta i}} \qquad (3.2)$$

where $v_{\theta i}$ is the tangential component of the velocity of the particles of size i at the sampling point.

In order to determine the conditions for taking a true sample, a series of samples was taken at various sampling times and sampling rates. The time was varied by operating the probe at different speeds, while the sampling rate was altered by applying different suctions to the inner tube of the probe.

Three samples were initially taken in every sampling position along lines D, E and F marked in Fig. 10. At each of these positions, one sample was taken for the shortest possible sampling time - about 10 ms - with the inner sampling tube at atmospheric pressure. A second sample was taken at the same pressure for a longer period of time. A third sample, still in the same position, was taken for approximately the same period of time as the second sample, but at

a higher suction rate - normally 0.38 atm.

The size analyses of these samples (Appendix 4) show that with the exception of positions D7 and E7 the three size distribution curves of the samples taken in the same location lie within a band with a maximum width of ± 1 to ± 4 percent on a cumulative basis. It was also noticed that the relative position of the three curves changed from one location to another showing no significant preference with regard to the sampling conditions.

In positions D7 and E7 it was found that the cumulative size distribution curves for the minimum sampling time differed by up to 40 percent from the other two which were close to each other. This anomaly was investigated by taking further samples in three specific locations, D4, D7 and E5, for different sampling times and at atmospheric pressure.

Once more, a marked effect of sampling time was manifest only in position D7 near the cyclone axis. The cumulative size distribution curves of the samples taken in this location (Fig. 12) show that the curves are grouped in two separate bands, divided according to sampling time. This suggested that the disturbance reached the sampling position in that location, within the range of times used. This effect was not observed in the other two positions except when the sampling period was several times longer than those generally used in the tests, for example, in position E5 with 4812 ms. The localised character of the effect near the cyclone axis may be due to a local phenomenon such as disruption by the air core.

It can be concluded that the stability of the size distribution of all samples taken in locations away from the axis proves that the curves obtained at the minimum sampling time represent a stable situation. In this sense, the results are comparable from point

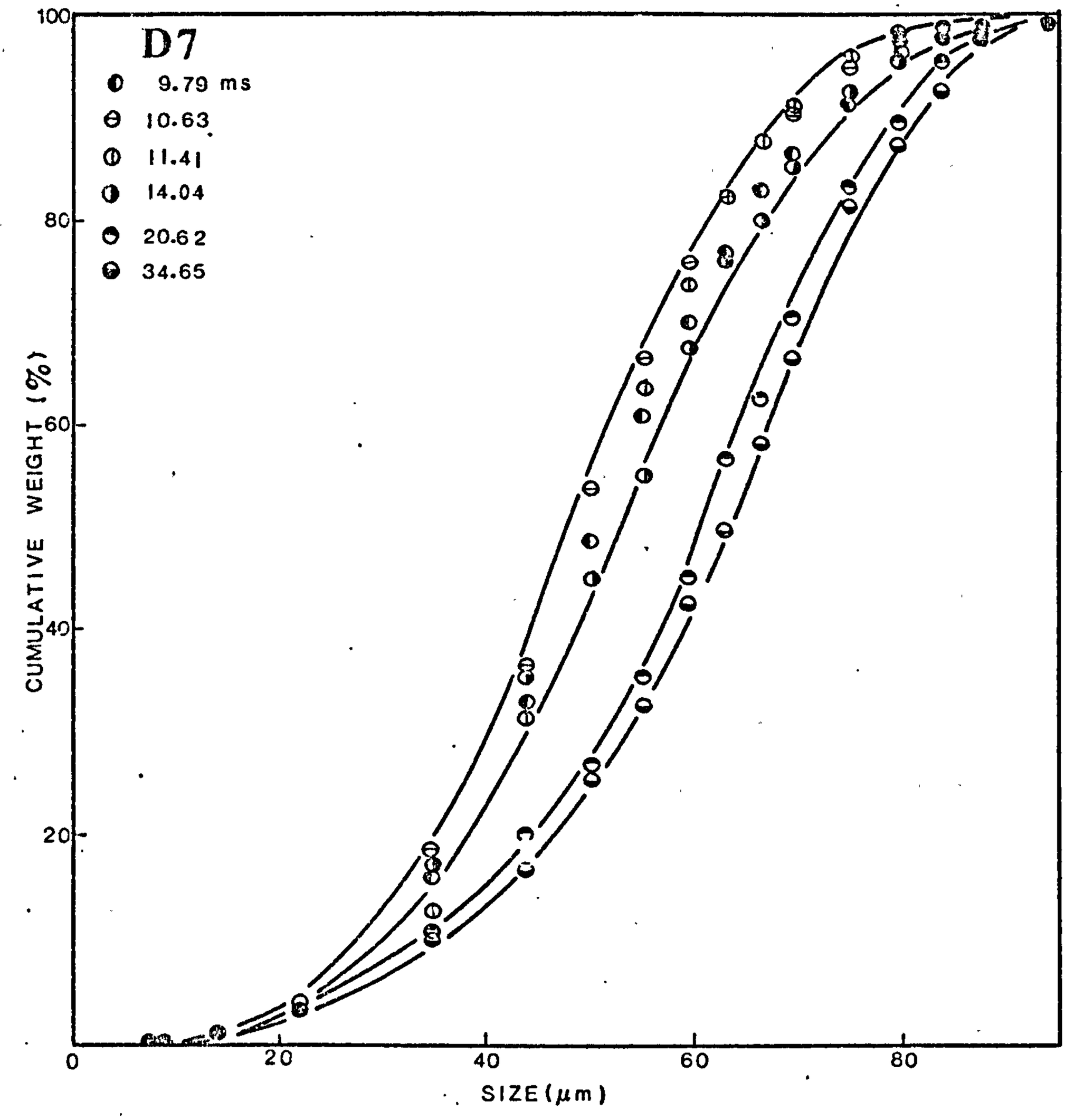

Fig. 12. Effect of sampling time in the size distributions of samples taken at position D7.

to point.

In addition, it was found that when the sampling positions approached the cyclone inlet and outlets, the sample size distribution approached the distribution of the corresponding input or outputs. It can be concluded that the stable configuration represented by the samples corresponds to the true configuration in the hydrocyclone.

Consequently, all the remaining sampling tests were executed at the minimum possible sampling time, with the inner tube at atmospheric pressure.

3.7. Results

The size distribution of all sampling tests are given in tabular form in Appendix 4 together with all conditions of the tests.

In addition, the ratio between the size frequency distributions of the samples taken at minimum sampling times and the size frequency distribution of the cyclone contents are shown graphically in Figs. 13 to 18 for the locations on lines A to F. The frequency distributions were derived from a polynomial fitted to the cumulative distribution by the method of least squares.

Table 1 includes the size distribution of the entire cyclone contents. This was obtained by averaging the distributions of two tests that were specifically performed for that purpose, as described in Appendix 3A.

3.8. Assessment of the Reliability of the Results

The consistency of the sampling experiment as a whole depends in the first place on how accurate the cyclone operation was reproduced from run to run. In order to assess the reproducibility

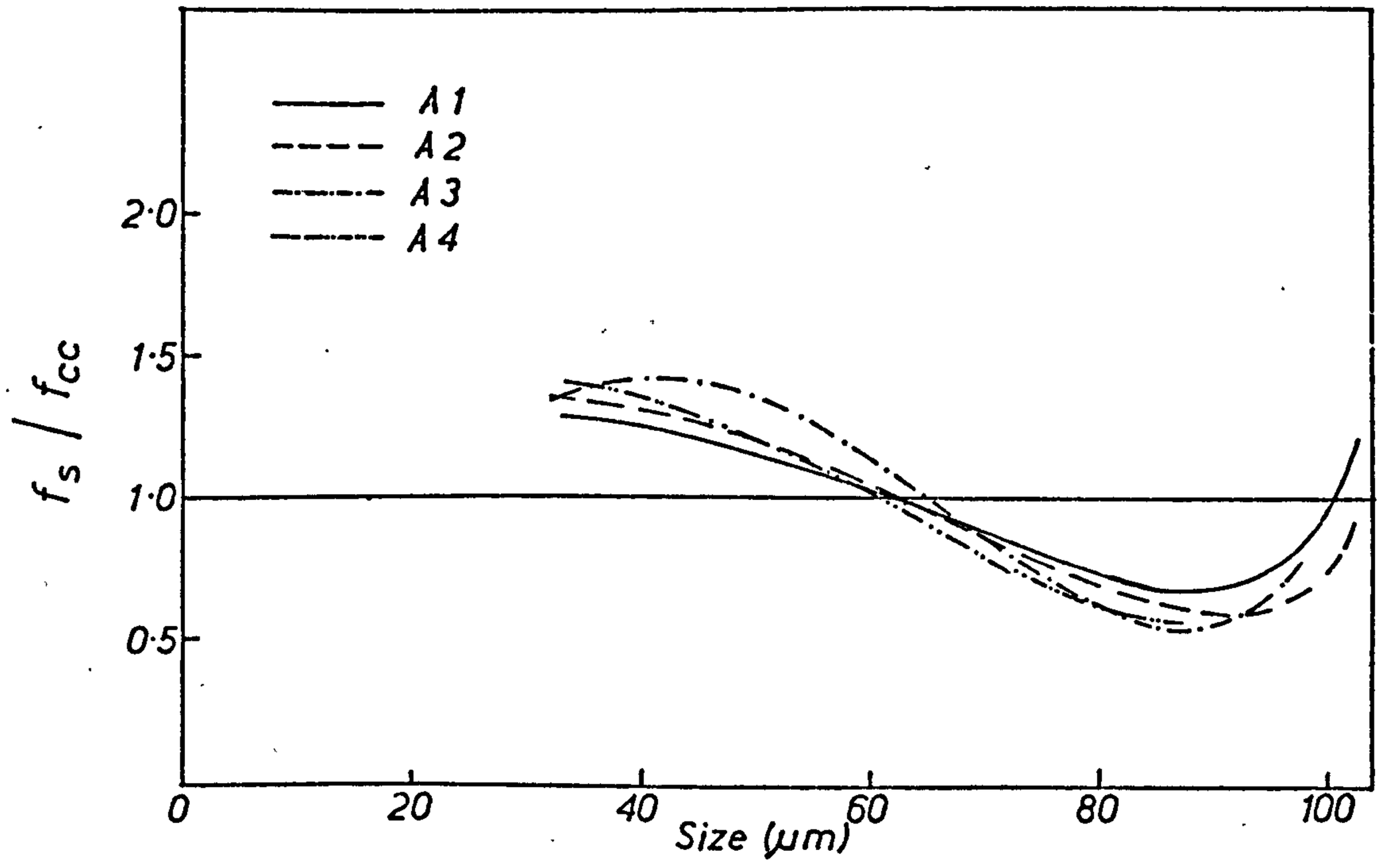

Fig. 13. Ratio between the retained size distribution of samples f_s and the cyclone contents f_{cc} : Level A.

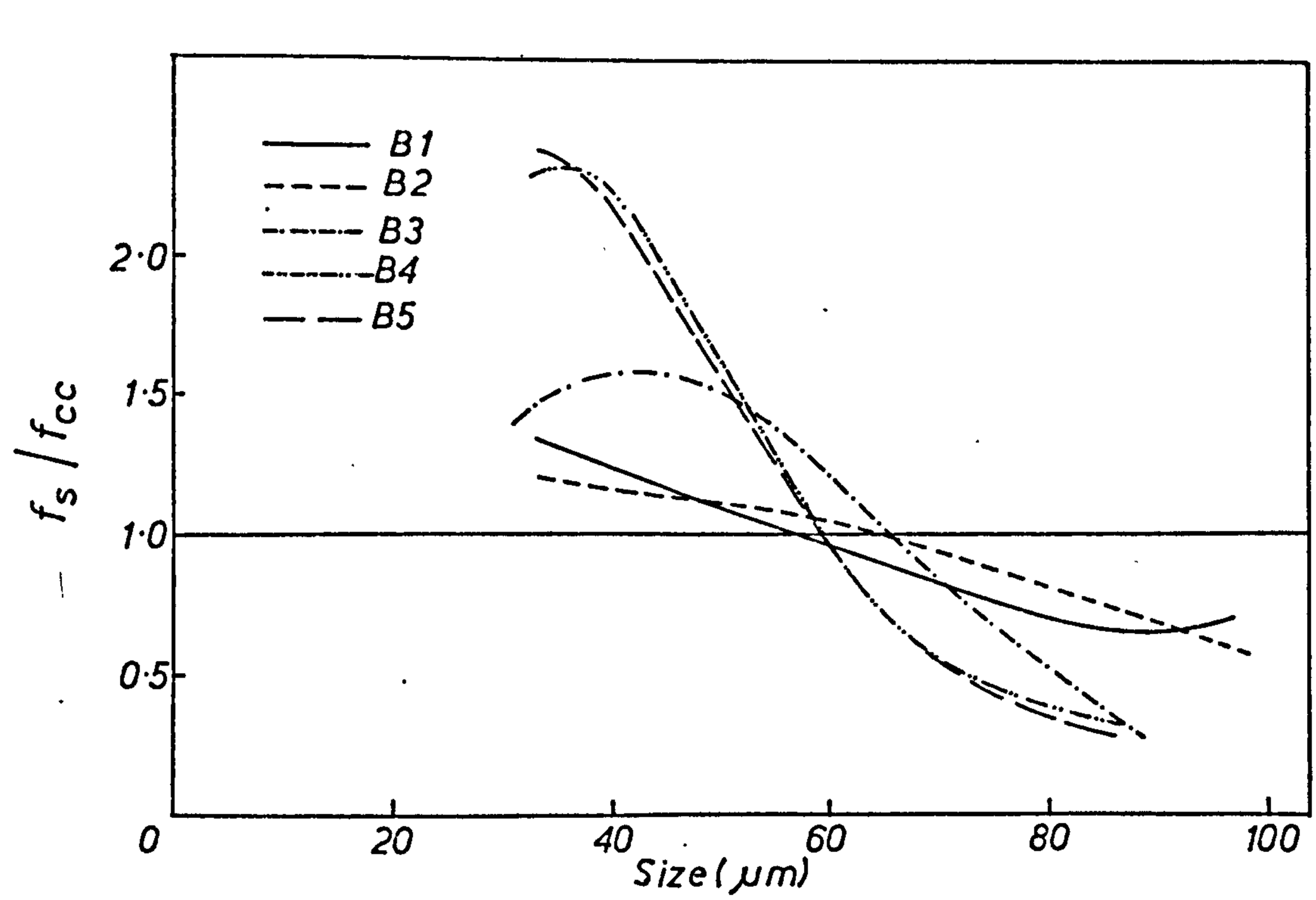

Fig. 14. Ratio between the retained size distribution of samples f_s and the cyclone contents f_{cc} : Level B.

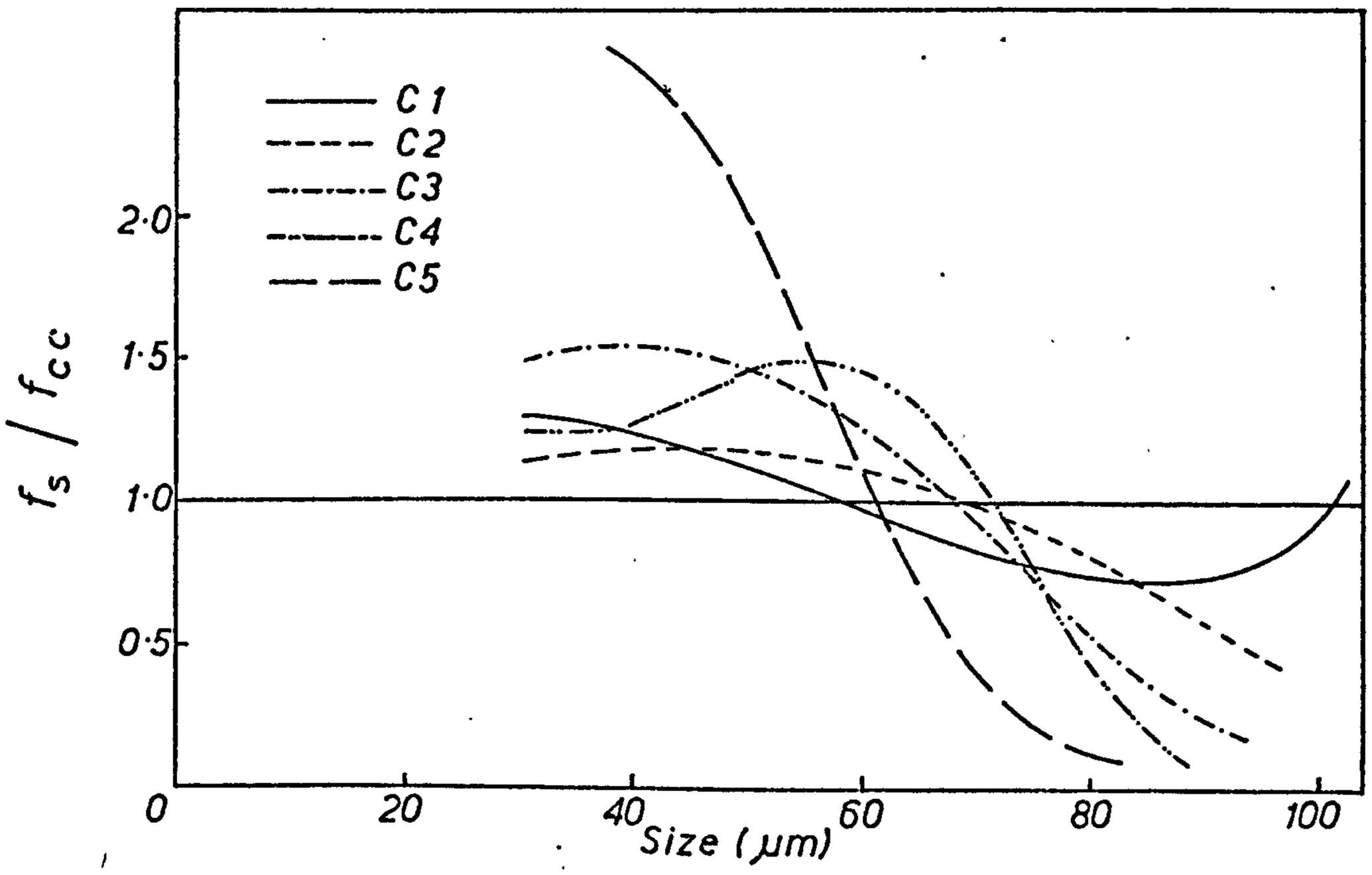

Fig. 15. Ratio between the retained size distribution of samples f_s and the cyclone contents f_{cc} : Level C.

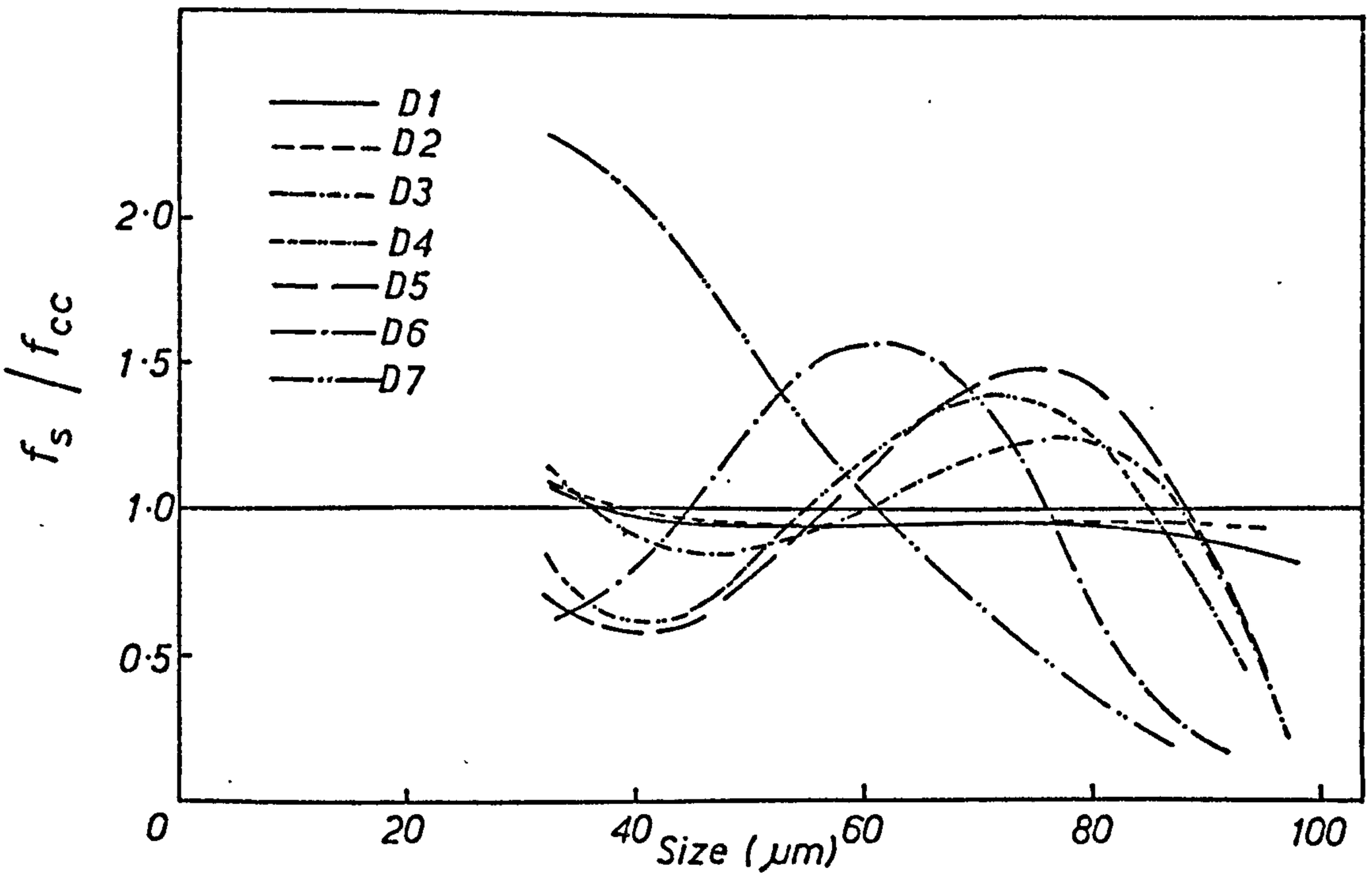

Fig. 16. Ratio between the retained size distribution of samples f_s and the cyclone contents f_{cc} : Level D.

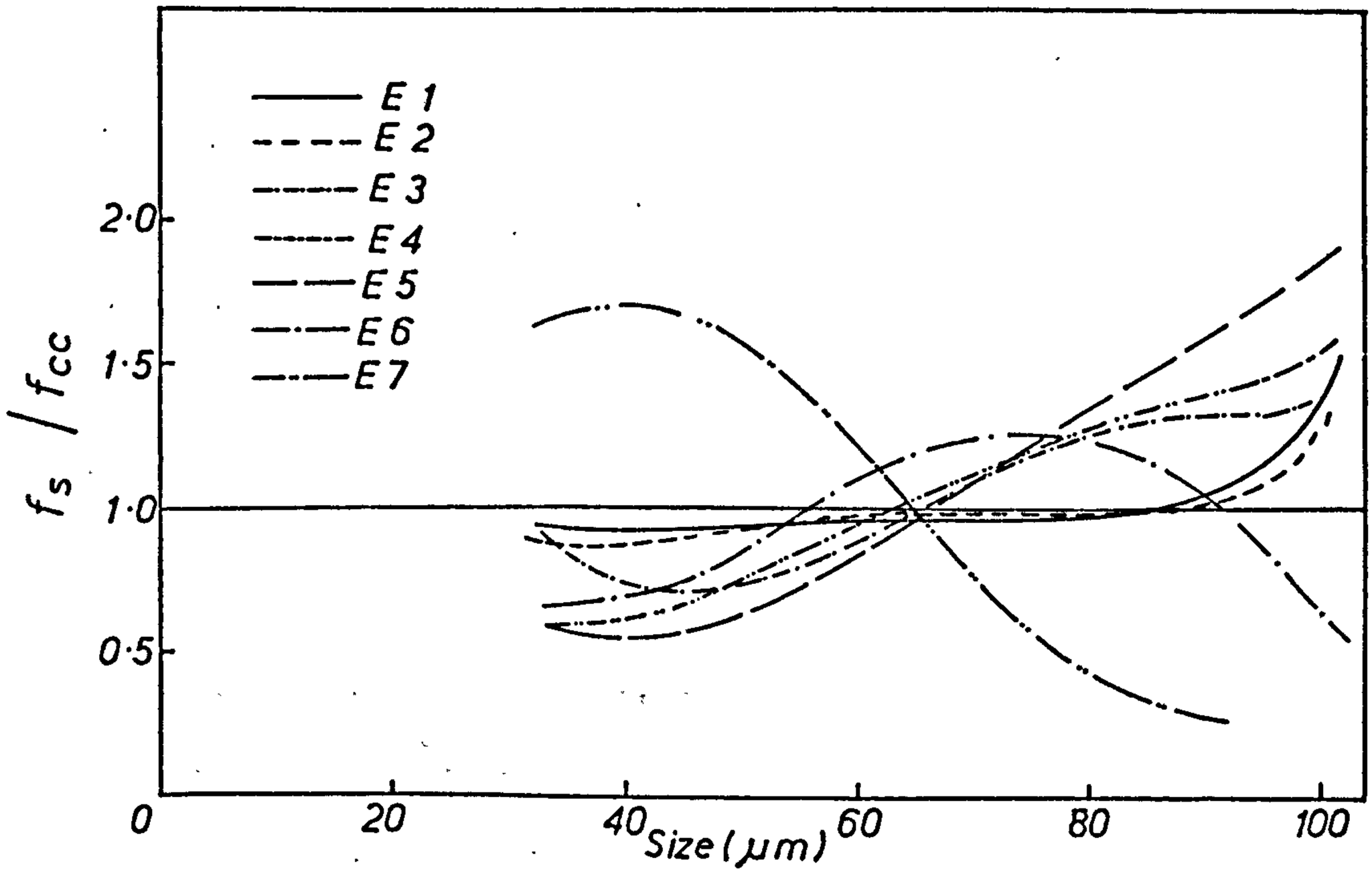

Fig. 17. Ratio between the retained size distribution of samples f_s and the cyclone contents f_{cc} : Level E.

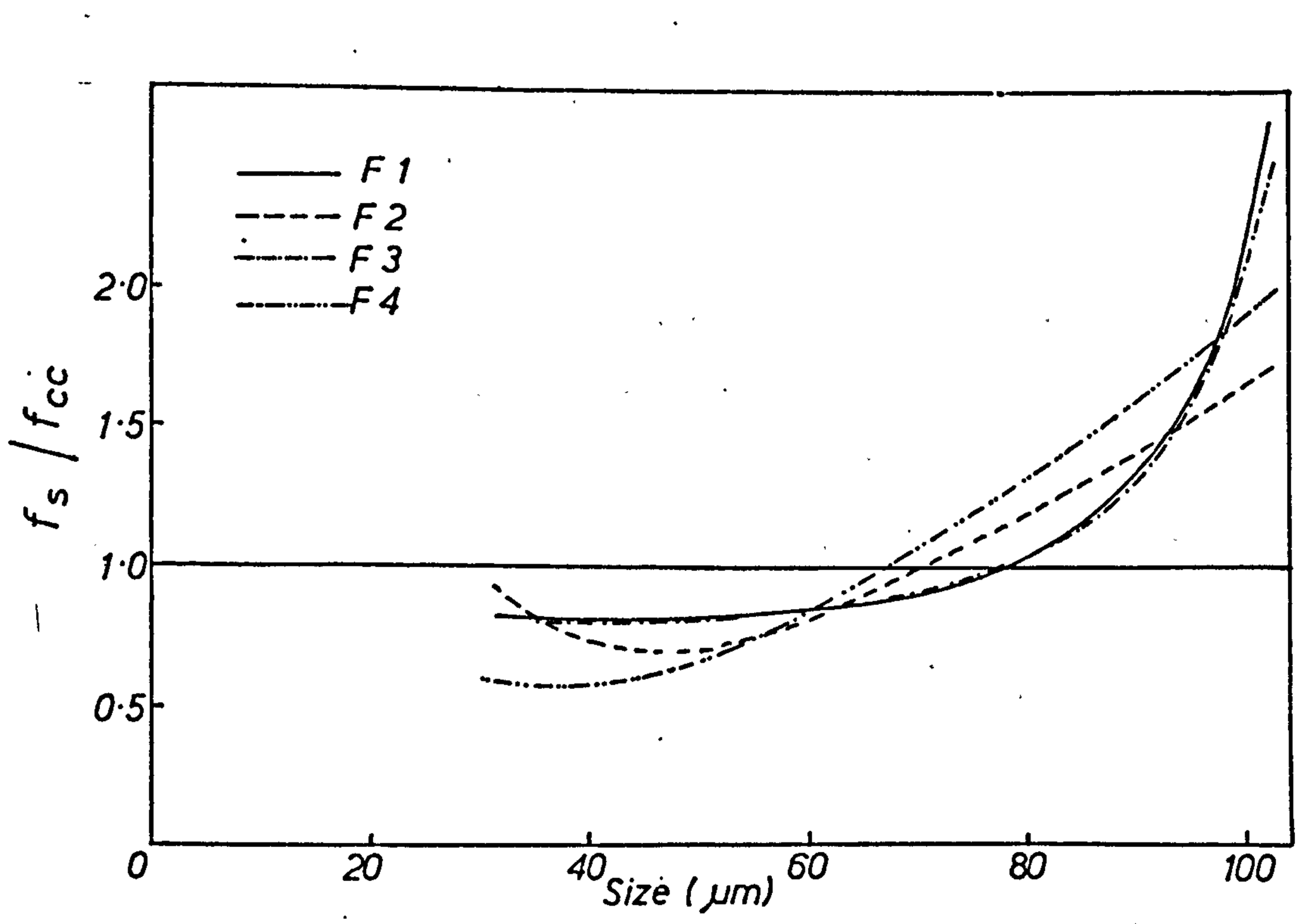

Fig. 18. Ratio between the retained size distribution of samples f_s and the cyclone contents f_{cc} : Level F.

of the cyclone conditions, underflow and overflow samples from 8 randomly selected tests were size analysed and in almost all tests the proportions of total feed solids and liquid that went to each product were determined. Thus, it was possible to estimate the variation of the conditions statistically (Table 1). The standard deviations are a measure of the reproduction errors, including all the errors involved in the experimental determination and subsequent computation of the data.

Random electrical interferences in the Coulter counter were more significant at high currents (small particle sizes). For this reason, the apparent variability is greater in the overflow distribution than in the underflow. Another characteristic of the sizing method is that, in calculating size distributions, the total amount of sample is obtained by adding the contributions of all size fractions. Therefore, the error at any size level is propagated over the whole distribution. Thus, frequency distributions derived from the cumulative data must be significatively in error for size fractions which represent proportions of the total weight that are comparable with the propagated error. This is generally the case with the upper and lower extremes of the size range. Excepting these extremes, the size distributions of the cyclone feed and products are reasonably well reproduced considering that the main interest was detection of variations in the spatial size distributions within the cyclone which are much more marked than errors in the external conditions.

In estimating errors in the size distribution of the samples taken with the probe, it is difficult to separate the effect of variations in the cyclone conditions from errors that arise only from withdrawal and analysis of the samples. However, an overall

estimation of the confidence limits for the final numerical results is obtained by comparing size distributions of samples taken in the same location when the conditions for taking a true sample were satisfied. As described in section (3.6), the maximum differences in those cases were between $\pm$ 1 to $\pm$ 4 percent of the total weight, on a cumulative basis. These figures, also affected by the errors due to the limitations of the sizing method mentioned above, are similar to those obtained in the analysis of the cyclone products.

Again, the errors in the numerical determination of positional size distributions are small enough not to be confused with the overall, larger variations across the cyclone. It should be noted that this investigation has been concerned only with general size distribution patterns and in no way relates to absolute values.

CHAPTER 4

DISCUSSION. COMPARISON OF CYCLONE THEORY WITH EXPERIMENT

4.1. Introduction

The criterion commonly used for assessing the quality of mathematical formulations of the cyclone classifier is the comparison between calculated classification cut sizes (d_{50}) and the corresponding experimental values. There are two simple reasons for using this criterion. Firstly, the cut size is often the only factor of practical interest and, secondly, it is relatively easy to obtain experimentally.

However, the exclusive use of the cut size for testing a model provides little information on why attempted formulations have so far generally failed to give correct predictions of cyclone performance and why some models succeed in giving the right answer for limited ranges of design and operational variables.

The data on positional size distributions within the hydrocyclone offer a novel and appropriate basis for judging whether any cyclone theory is sufficiently well founded to cover all features of cyclone behaviour.

4.2. Effect of ignoring recirculation and short circuit flow

In most attempts at theoretical formulation, the analysis of the motion of solid particles has been simplified by ignoring flow recirculation in the bulk of the cyclone as well as short circuit flow near the cyclone roof to the vortex finder. The mathematical model developed here (Chapter 2) can be regarded as a characteristic

example.

A consequence of these simplifications is a marked difference between particle flow patterns calculated from the model (Fig. 4) and those inferred from experiments (Fig. 23, Chapter 5). The disagreement between reality and model is exhibited in a more definitive way when the positional size distributions obtained experimentally are compared with those computed from the model. In order to present the calculated values in a form comparable with the experimental results given in Figs. 13 to 18, Fig. 19 shows ratios of the size distributions calculated as described in section (2.9) with the size frequency distribution of the actual cyclone contents taken as a given standard. As seen in Eq. (2.18), the tangential component of the velocity of the particles is independent of the particle size, thus f_{pi} given by Eq. (2.41) is equivalent to the distribution $f_{\theta i}$ obtained experimentally given by Eq. (3.2).

The curves derived from the model tend to a maximum at the particle size with its equilibrium orbit coinciding with the point where each curve is calculated. Particles larger than that specific size are not present in the position considered and, therefore, the curves drop discontinuously to zero after the maximum. The coordinates of the positions where the computations were performed are tabulated in the same figure, together with the corresponding largest size present. The sum of all sizes needed to calculate the frequency distributions in Eq. (2.42) was estimated from only a small number (5-10) of sizes, hence there may be some vertical displacement of the curves in the figure.

The pattern of size distributions calculated from the model, which is similar in all cyclone levels, differs from the patterns of all the levels examined experimentally. In particular, the actual

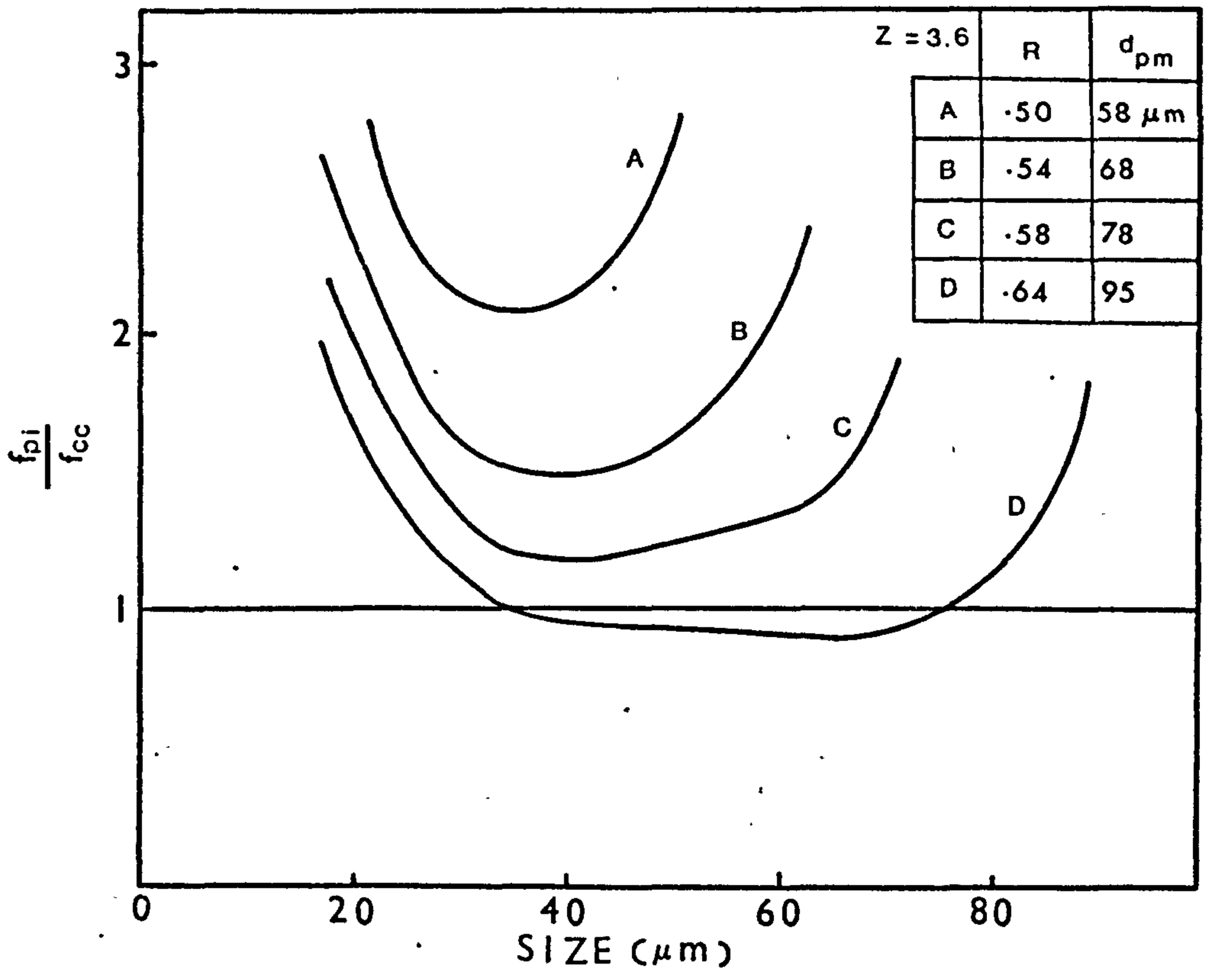

Fig. 19. Ratio between retained size distributions calculated from the model and the actual cyclone contents.

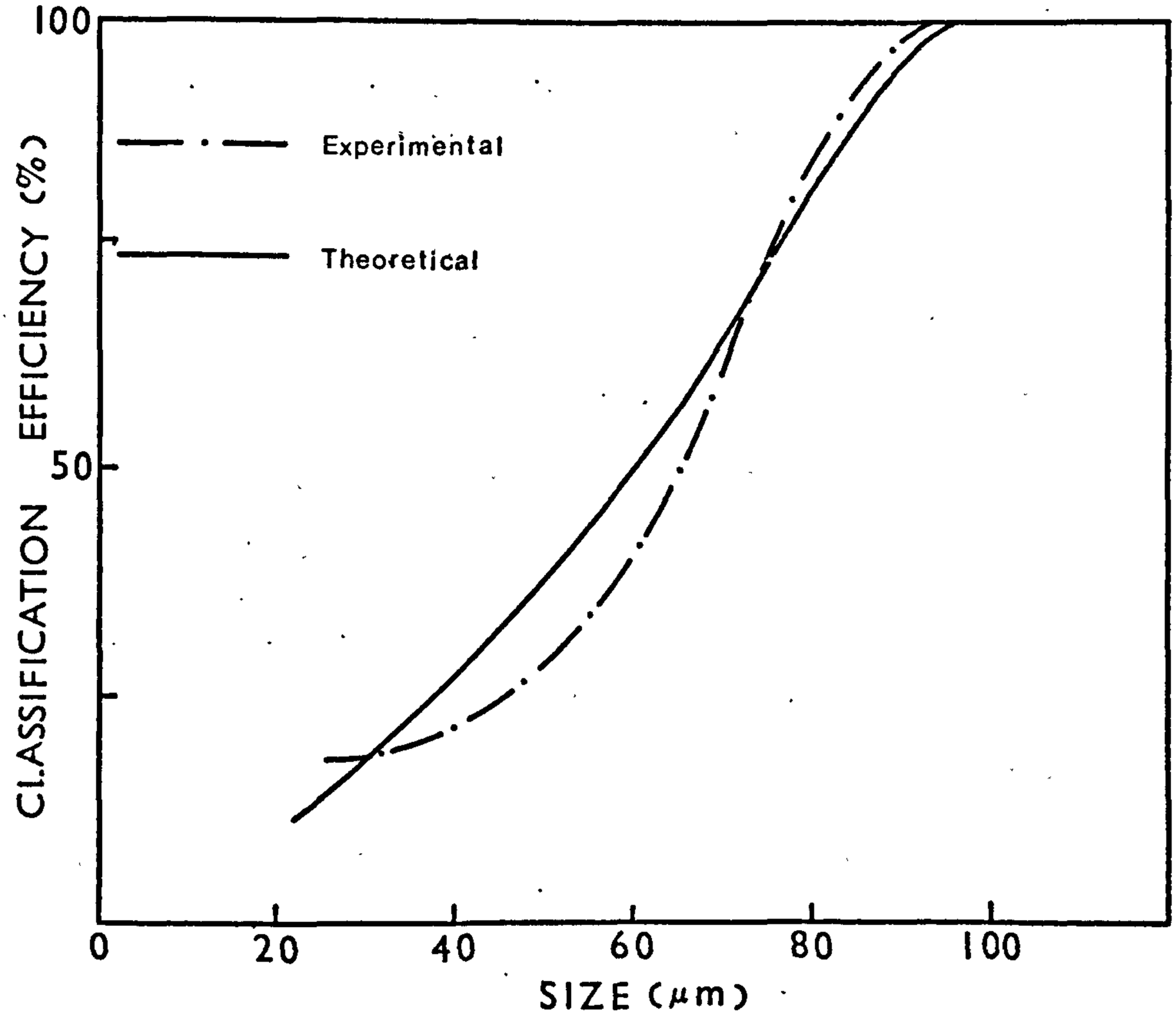

Fig. 20. Experimental and theoretical classification efficiency curves.

presence of particles of all sizes, in almost all positions radially across the cyclone, indicates the non-existence of the equilibrium orbits predicted by the model.

One feature common to the model and the experiments is that the relative proportion of fine material tends to increase towards the axis, while the proportion of coarse material increases towards the apex. This is reflected in the fact that the motion of particles in the model results in a size classification which closely resembles the corresponding experimental one (Fig. 20).

A partial reconciliation is found if it is assumed in the model that some of the particles which reverse their axial velocity miss the vortex finder and enter temporarily into a recirculation zone in which they are in better positions to be eventually captured by the overflow pipe or return to the downward stream.

According to this assumption, particles which enter the recirculation region have already experienced a primary stage of classification. The main function of the recirculation zone may then be to provide opportunities to particles which are misplaced by collisions or turbulence to regain their classified paths.

A more realistic model should include recirculation and short circuit flows. Because of the difficulties in obtaining a complete solution of the Navier - Stokes equation, simplified models to include these flows were studied, but the attempts proved unsuccessful. It was found that the potential flow of a vortex pair behind a cylinder in a uniform stream presents an interesting analogy with the main conjectural flow in an axial plane of a cyclone (Fig. 21), but the combination of a pattern of this type with a vortical motion in the azimuthal direction is not feasible.

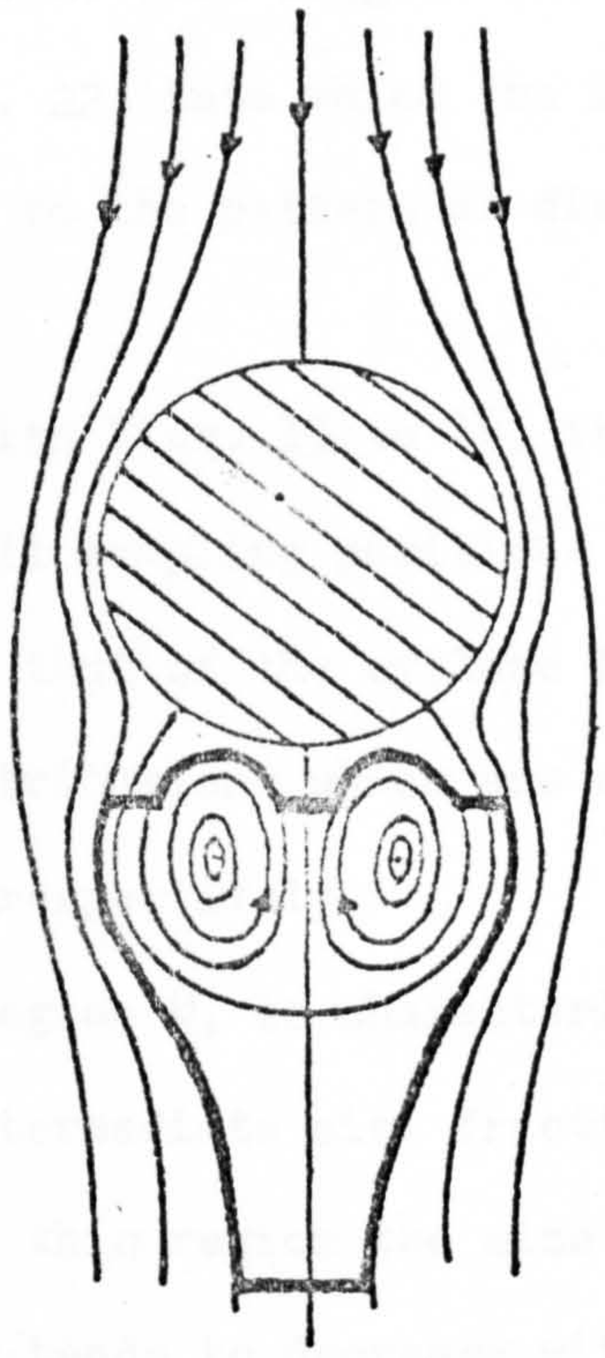

Fig. 21. Sketch of the flow of a vortex pair behind a cylinder in a uniform stream, showing the cyclonic contour (in heavy line).

CHAPTER 5

BEHAVIOUR OF SOLID PARTICLES WITHIN THE HYDROCYCLONE

5.1. Patterns of the Size Distributions within the Hydrocyclone

The results of the test work suggest the existence of four regions, sketched in Fig. 22, into which the interior of the cyclone may be divided according to the pattern of distribution of particle sizes.

Comparing Fig. 11 with Figs. 13 to 18, it can be observed that region A contains all sampling positions that show size distributions similar to that of the cyclone feed. Equally, regions B and C present size distributions which are similar to the cyclone underflow and overflow, respectively.

The central zone, region D, is characterized by higher concentrations of the intermediate size fractions than the whole cyclone contents. Across this region the size fraction that appears with a maximum frequency tends to decrease with the radial distance from the axis.

5.2. Qualitative Analysis of Particle Behaviour in the Hydrocyclone

In attempting an explanation of the size distribution pattern, it may be noted first that only the material in region D appears to be being subjected to a classification process. In the remaining cyclone space, there are either no classification effects, as in region A, or classification is already completely developed, as in regions B and C. In particular, it is important to note that most of the conical section of the cyclone appears to play no direct role in the classifying action.

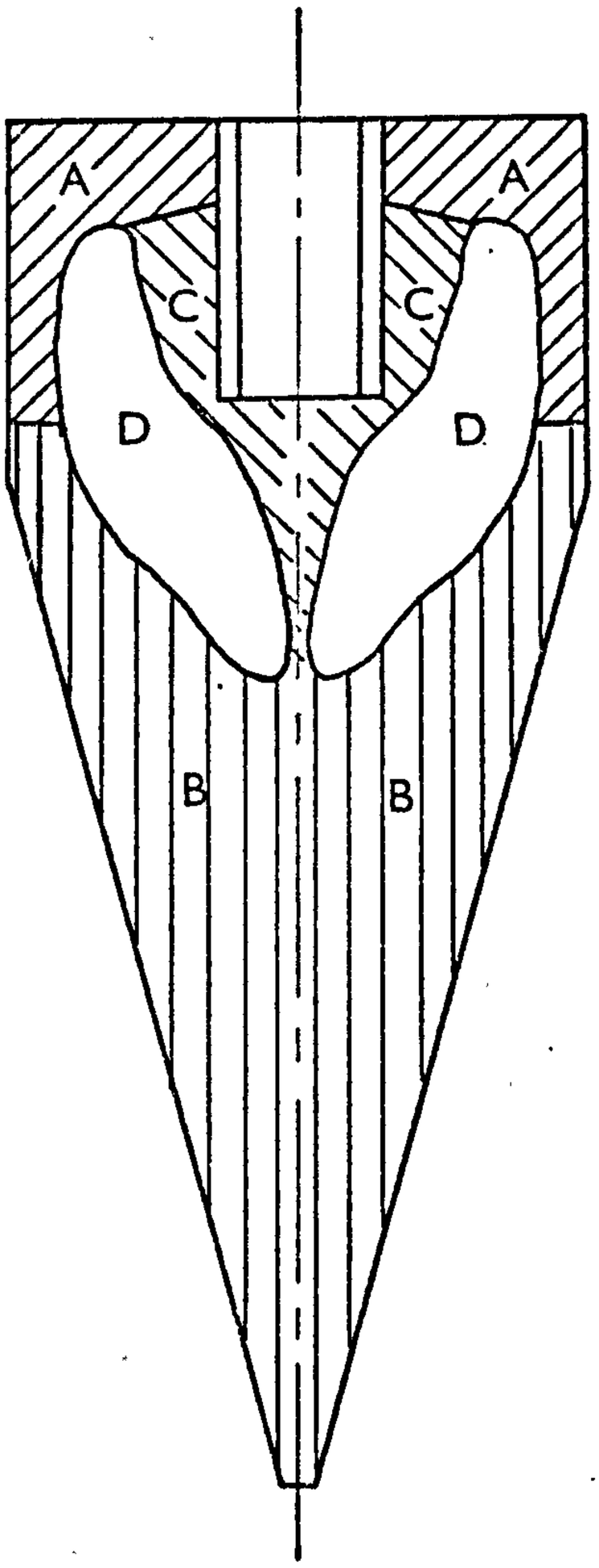

Fig. 22. Regions of similar size distributions within a hydrocyclone.

The absence of classification effects in region A suggests that immediately after entry the feed flow is dispersed all around the cyclone in this region. High speed cine film, taken previously in this laboratory to observe the motion of solid particles in a glass cyclone, provides visual evidence that at the entry level the tangential feed flow is diverted into orbital motion by the cyclone wall and forms a spiral that reduces its diameter by advancing to the outside of the vortex finder pipe. The preference of the feed flow to move initially across the top region may be due to the constraining effect of the recirculating flow just under this region.

Once the particles are within region A, they must be continuously displaced by newly entering feed. The particle size distributions across the cylindrical section outside region A suggests that a classifying action results in three streams : one from region A to region C along the vortex finder wall containing a high proportion of fine material; another, from region A to region B along the cylindrical wall carrying the majority of coarse particles; and a third stream from region A to region D with a high proportion of the middle size particles of the feed.

Cohen et al. [13] pointed out that the ratios between the size frequency distributions of the cyclone contents and the feed are proportional to the mean residence times of the individual size fractions in the cyclone. They further showed that the middle size particles remain inside the cyclone for longer periods of time than the finer and coarser fractions. This observation was verified with the present conditions, as shown in Fig. 11. Since the intermediate size fractions are segregated in region D of the cyclone, they must stay there for relatively long times. This can be explained with the generally accepted idea, based on observations

and measurements by Kelsall [3] and Bradley and Pulling [4], that there is a secondary toroidal vortex in that region where the particles can be subjected to recirculatory motion. These particles pass into region C (and the overflow) or region B (and the underflow) according to their radial segregation in region D.

The longest residence time is that of particles coarser than d_{50} since they pass predominantly into the relatively large cone volume of region B. Particles of d_{50} size and smaller pass into the restricted volume of region C and leave the cyclone more quickly. This is consistent with the measured longest residence times for particle size approximate to the d_{70} size.

The inactive nature of the conical section in relation to the classifying process indicates a difference in cyclone behaviour with a slurry and with water only. Bradley's observations with water showed that most of the overflow volume has to move well down the cone to be able to flow radially across the locus of zero axial velocity. This would suggest that the size sorting of most of the solid particles occurs in the lower region of the cyclone. However, the present results indicate that the determining size separation takes place in the upper regions of the cyclone and that the solids in the cone are already classified. The reason for this difference might be that, when solids are added, the restricted discharge capacity of the apex orifice causes underflow material to become increasingly concentrated in the cyclone cone, thus diminishing the flow of the slurry there. Consequently, it is reasonable to expect the determining classifying process to occur outside the cone.

Alternatively, it might be argued that the flow rate of the transverse circulation is too low to produce a fluid drag large enough to dislodge solid particles from their inertial orbital paths

in the cone.

Fig. 23 is a schematic representation of the flow patterns of different size fractions which might produce the size distribution pattern obtained in this investigation. This flow configuration somewhat resembles that suggested by Bradley; the basic difference is that here the sorting path lines are more confined to the cylindrical section of the cyclone.

Cohen et al. found that poor classification yields a flat curve of residence time distribution. This indicates a poorly--developed or lacking zone D. This defect may be caused by a variety of operating conditions and design factors. For example, excessive pulp density in the feed may cause congestion in zone D; low feed rates, relative to the contained volume of a cyclone, may fail to generate a well-developed zone D; absence of the vortex finder pipe would cause zone D to "leak out" at the top; and a cyclone of insufficient axial height (excessively wide cone angle) would allow zone D to "leak out" through the apex.

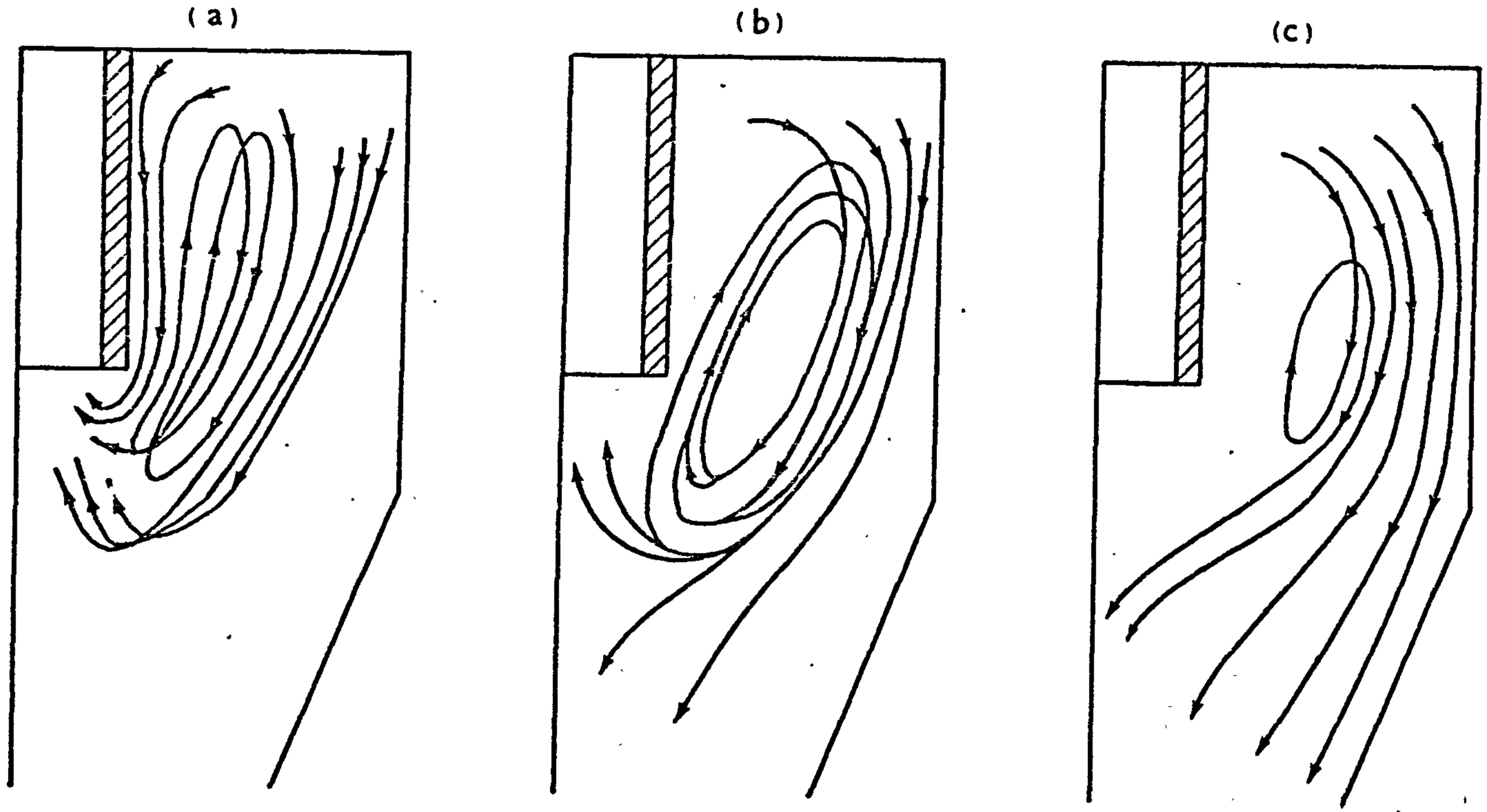

Fig. 23. Schematic representation of the flow pattern of particles of: (a) fine size, (b) middle size and (c) coarse size.

CHAPTER 6

CONCLUSIONS

The high speed sampling technique can be successfully used for determining positional size distributions within a hydrocyclone operated under normal conditions.

The classification efficiency curve calculated from a model based on the motion of particles in a fluid field that simulates only the main cyclone flow closely resembles the classification efficiency curve obtained in the tests. The patterns of positional size distributions calculated from the theoretical model, differ from the patterns obtained from measured size distributions. The disagreement between model and experiment might be due to absence in the model of recirculation and short circuit flows.

The measured size distributions are interpreted by division of the interior of the cyclone into four regions of similar size distribution patterns. Unclassified feed is distributed all across the top region of the cyclone; most of the cone exhibits size distributions that are similar to the underflow distribution; the space surrounding the vortex finder pipe contains fully classified overflow particles; and only a toroidal central region appears to be the locus of a classifying process in action. The size fractions in the central region are radially distributed so that decreasing sizes show maxima at decreasing radial distance from the axis.

The size distribution pattern is explained by the assumption of a toroidal vortex in the central region. This is consistent with patterns of residence times.

The conclusion that the cyclone cone plays no direct role in

the classification process indicates differences in cyclone behaviour with a slurry and with water only.

APPENDIX 1

APPROXIMATE ANALYTICAL SOLUTION OF THE EQUATION

$$y\left(\frac{dy}{dx} + 1\right) = k\left(\frac{1 - x^4}{x^3}\right)$$

Setting $X = R$, $Y = \frac{dR}{dT}$, Eq. (2.19) can be expressed by:

$$Y \frac{dY}{dX} + AY = \frac{C}{X^3} - BX \tag{1}$$

The simplest form of this equation is:

$$y\left(\frac{dy}{dx} + 1\right) = k\left(\frac{1 - x^4}{x^3}\right) \tag{2}$$

where:

$$y = A\left(\frac{C}{B}\right)^{1/4} Y$$

$$x = \left(\frac{C}{B}\right)^{1/4} X \tag{3}$$

$$k = \frac{B}{A^2}$$

If x_0 is any fixed value of x and $\psi = x - x_0$, then:

$$y\left(\frac{dy}{d\psi} + 1\right) = \frac{k}{x_0^3}\left(1 + \frac{\psi}{x_0}\right)^{-3} - kx_0\left(1 + \frac{\psi}{x_0}\right) \tag{4}$$

Expanding $\left(1 + \frac{\psi}{x_0}\right)^{-3}$ in Taylor's series around $\psi = 0$ and assuming $\frac{\psi}{x_0} \ll 1$ so that terms in powers higher than 1 can be neglected, hence:

$$y\left(\frac{dy}{d\psi} + 1\right) = \frac{k}{x_0^3}\left(1 - 3\frac{\psi}{x_0}\right) - kx_0\left(1 + \frac{\psi}{x_0}\right)$$

$$= \frac{k}{x_0^3} - kx_0 - \left(\frac{3k}{x_0^4} + k\right)\psi$$

$$= k_1 - k_2\psi \qquad (5)$$

where

$$k_1 = \left(\frac{1}{x_0^3} - x_0\right)k \qquad (6)$$

$$k_2 = \left(\frac{3}{x_0^4} + 1\right)k$$

Putting $y = \phi(k_1 - k_2\psi)$, (7)

then:

$$dy = (k_1 - k_2\psi)d\phi - k_2\phi d\psi$$

Substituting this into Eq. (5) and separating terms in ϕ and ψ, gives:

$$\frac{\phi d\phi}{k_2\phi^2 - \phi + 1} = \frac{d\psi}{k_1 - k_2\psi} \qquad (8)$$

which, after integration takes the form:

$$\frac{1}{2k_2}\ln(k_2\phi^2 - \phi + 1) + \frac{1}{2k_2\sqrt{1 - 4k_2}}\ln\frac{2k_2\phi - 1 - \sqrt{1 - 4k_2}}{2k_2\phi - 1 + \sqrt{1 - 4k_2}}$$

$$= -\frac{1}{k_2}\ln(k_1 - k_2\psi) + C_1 \qquad (9)$$

where C_1 is the integration constant whose value can be determined by substituting the initial conditions.

Eq. (9) can be modified to the form:

$$\frac{(k_2\phi^2 - \phi + 1)(2k_2\phi - 1 - k_3)^{\frac{1}{k_3}}}{(2k_2\phi - 1 + k_3)^{\frac{1}{k_3}}} = \frac{C_0}{(k_1 - k_2\psi)^2} \qquad (10)$$

where:

$$k_3 = \sqrt{1 - 4k_2} \quad ,$$

and

$$C_0 = e^{2k_2C_1}$$

The solution of Eq. (8) given by Eq. (10) is valid when $\frac{\psi}{x_0} \ll 1$, so it is permissible to set $\psi = 0$ while letting x_0 take all its possible values, that is $x_0 = x$. Hence, from Eqs. (6),

$$k_1 = (\frac{1}{x^3} - x)k$$

$$k_2 = (\frac{3}{x^4} + 1)k$$

and from Eq. (7).

$$\phi = \frac{y}{k_1}$$

Thus, Eq. (10) is an approximate solution of the differential Eq. (2). Owing to the implicit form of Eq. (10), it is necessary to evaluate y as a function of x by a numerical method.

In solving Eq. (2.19) using these results, the method of successive bisection was applied to evaluate y from Eq. (10) and then the second integration was obtained using Trapezoid Rule. The final result that gave R as a function of time T agreed perfectly with the solution obtained by the method described in Chapter 2.

APPENDIX 2

THE BEHAVIOUR OF THE CHARACTERISTIC SIZE FRACTION IN SAMPLING THROUGH AN ASPIRATED NOZZLE

In sampling a slurry through an aspirated nozzle there is a characteristic size fraction whose relative proportion in the sample is independent of the sampling velocity, remaining equal to its proportion in the stream being sampled.

To show this set:

V_0 : velocity of the stream at the sampling point when the probe is not there.

V_s : sampling velocity.

m_i : mass of particles of size i that enter the nozzle in the unit of time when $V_s = V_0$.

m_{si} : mass of particles of size i that enter the nozzle in the unit of time at sampling velocity V_s

$$M = \sum_i m_i \quad : \text{ and } \quad M_s = \sum_i m_{si}$$

If $V_s > V_0$, then the flow converges into the orifice and the size distribution in the sample will be finer than the true one, because coarse particles will tend to follow their initial paths due to their higher inertia.

If $V_s < V_0$, then the flow will diverge as it approaches the orifice. Finer particles will tend to be dragged away from the orifice more effectively than coarser ones and, therefore, the size distribution of the sample will be coarser than the true one.

If $V_s = V_0$, i.e., if the sample is isokinetic, then the sample

will be true in its size distribution.

In brief:

if $\frac{V_s}{V_0} > 1$ then $\frac{m_{si}}{m_i} > 1$ and $\frac{M_s}{M} > 1$;

if $\frac{V_s}{V_0} < 1$ then $\frac{m_{si}}{m_i} < 1$ and $\frac{M_s}{M} < 1$;

if $\frac{V_s}{V_0} = 1$ then $\frac{m_{si}}{m_i} = 1$ and $\frac{M_s}{M} = 1$.

Thus, the size distribution ratio between sample and stream

$$\frac{f_{si}}{f_i} = \frac{\frac{m_{si}}{M_s}}{\frac{m_i}{M}} = \frac{m_{si}}{m_i} \cdot \frac{M}{M_s}$$

is the product of two quantities which are linked either so that one of them is greater than unity and the other smaller, or both are equal to unity. Therefore, there must be at least one size fraction for each sampling velocity for which the product is unity.

In moving from anisokinetic towards isokinetic sampling, the sample approaches the size distribution of the stream. Therefore, if for any isokinetic sample the proportion of a size fraction in the sample is the same as in the stream, this will remain so at any sampling velocity.

The ratio between m_{si} and m_i can be expressed by [14]:

$$\frac{m_{si}}{m_i} = (1 - \alpha_i) \frac{V_s}{V} + \alpha_i \quad , \qquad \text{with} \quad 0 < \alpha_i < 1$$

where α_i , called the inertial parameter of the size fraction i, depends on the inertia of the particle and the flow pattern in the

neighbourhood of the nozzle.

Hence:

$$M_s = \sum_i m_{si} = \sum_i m_i \frac{V_s}{V} - \sum_i m_i \alpha_i \frac{V_s}{V} + \sum_i \alpha_i m_i$$

Dividing by M and ordering:

$$\frac{M_s}{M} = (1 - \bar{\alpha})\frac{V_s}{V} + \bar{\alpha}$$

where

$$\bar{\alpha} = \frac{1}{M} \sum_i \alpha_i m_i$$

With this, the size distribution ratio can be expressed by:

$$\frac{f_{si}}{f_i} = \frac{m_{si}}{m_i} \frac{M}{M_s} = \frac{(1 - \alpha_i)\frac{V_s}{V} + \alpha_i}{(1 - \bar{\alpha})\frac{V_s}{V} + \bar{\alpha}}$$

Therefore, $\frac{f_{si}}{f_i} = 1$ when $\alpha_i = \bar{\alpha}$. Thus, the size fraction that is sampled independently of the sampling velocity is the one whose inertial parameter corresponds to the weighted mean of all the inertial parameters.

Experimental Verification. Experimental sampling tests in a pipe were carried out under known conditions in order to confirm the above deductions. Experimental curves of size distribution ratio as a function of velocity ratio are shown in Fig. 24. Each of these curves was fitted by the method of least squares from 9 experimental points. The conditions of the tests are given in the same figure.

Near $\frac{V_s}{V_o} = 1$ the deviations of the size distributions of the

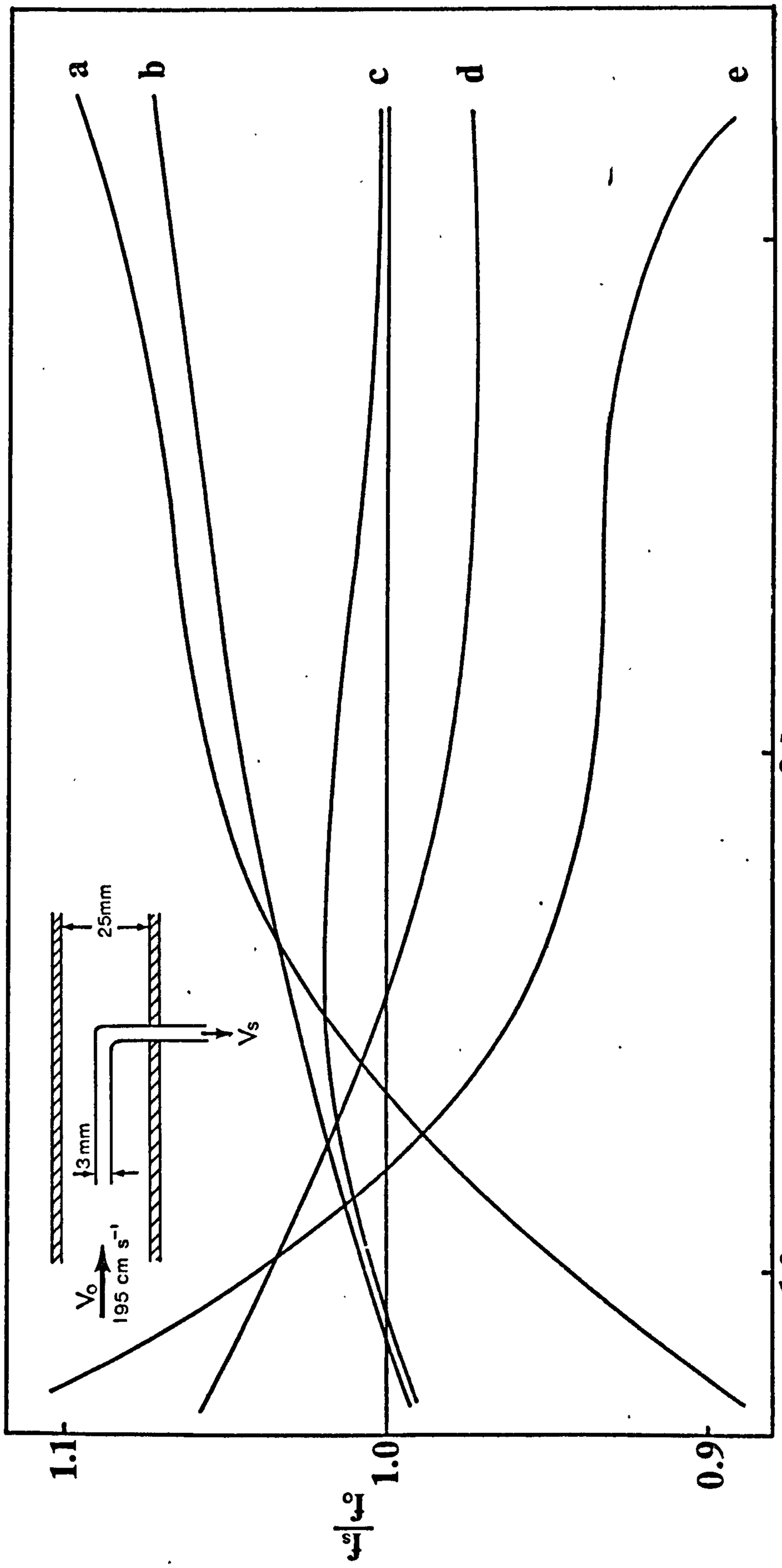

Fig. 24. Experimental size distribution ratio as function of velocity ratio.
a - 200 : b - 150 + 200 : c - 100 + 150 : d - 72 + 100 : e - 52 + 72 (BS mesh)

samples from those of the stream were comparable in magnitude with the errors involved in the experiment. Besides, the value V_o used is the mean velocity in the pipe, which should be an underestimation of the velocity in the centre of the pipe where the samples were taken. However, the trend appears to be in reasonable agreement with the previous reasoning.

APPENDIX 3

EXPERIMENTAL PROCEDURE

3.A. Test Procedure

Each run of the cyclone was started with water only, in order to check the electromagnetic flow-meter against the rotameter and to calibrate the γ-ray density gauge.

The sump was filled with water up to a fixed level and the pump started. A batch of sand was added and the flow rate adjusted to the required value. More water was added to the sump until the density of the slurry, observed in the density gauge, reached a predetermined value.

To prepare the sampling probe system, the probe was set for sampling at a chosen position; if necessary, the pressure in the inner tube was adjusted using the vacuum pump; the compressed air pressure was set at the value (estimated by experience) required for moving the probe at the desired speed; the microscope lamp was switched on; the position of the photo-transistor was adjusted so that light from the lamp could reach it exactly when the sampling orifice was opened; and the timer-counter was set to zero.

Once the cyclone circuit was running steadily at the desired flow rate and slurry density, simultaneous samples of the cyclone products were collected into two tared glass cylinders placed under the sample cutter. The sample slots were washed down with a weighed volume of water to ensure complete collection of the samples. The volumes of samples were chosen so that they contained about 100 g of solids.

The vessels containing the samples were weighed and the water

in them removed by decanting and drying. The solids were weighed and kept for eventual size analysis.

Immediately after sampling the cyclone products, the temperature of the slurry was measured with a mercury thermometer and the probe actuated by opening the compressed air valve. The cyclone was then rapidly switched out of the circuit to avoid splashing through the wall window.

The probe was withdrawn outside the cyclone, keeping the sampling orifice closed. The tubes were carefully sprayed with water to remove all the particles on them and within the opened tip. The inner tube was then connected to vacuum and the sampling orifice opened in water to wash down all particles of the sample into the bottle trap. The water used in this operation and in all subsequent dilutions of the sample came from a laboratory still and was sufficiently free of suspended solids to be used for the blank electrolyte for the Coulter counter.

To analyse the whole cyclone contents the cyclone circuit was run following the same procedure as above, but when steady state was reached the feed to the hydrocyclone was stopped by switching the pump off. Simultaneously, a bucket was inserted below the apex orifice to collect the entire contents of the hydrocyclone for analysis.

3.B. Size Analysis Procedure

All samples were size analysed using a "Model ZB Industrial" Coulter counter, following the instructions provided by Coulter Electronics Ltd., [15] whenever possible.

Some modifications of the standard procedure were needed for two reasons. Firstly, the size distributions of the samples were

too coarse to be kept well mixed by the built-in agitator of the Coulter counter. For the same reason, the flow through the orifice tube was too low to drag away particles that settled at the bottom of the orifice tube. Secondly, external radiation "noise" and line "noise" produced unacceptable background counts.

The mixing problem in the sample beaker was solved by using a strong agitator operated with compressed air. Entrainment of air bubbles into the sample was prevented by means of baffles.

The settling of particles at the bottom of the orifice tube was controlled by flushing the inside of the tube periodically. This was achieved by means of a three-way control piece in an arrangement (Fig. 25) that enables the auxiliary outlet of the orifice tube to draw a volume of clean electrolyte at high rate through the tube. The flushing action is obtained when A and B are opened (see Fig. 25), while C connects F with D. For normal operation, A is closed, while C connects G with D.

Electrical interference was substantially eliminated by locating the Coulter counter in a shielded room and by using an auxiliary mains filter and a voltage stabilising transformer.

In general, the number of particles in the volume of sample (400 cm^3) was larger than the maximum number needed for correct use of the Coulter counter. To sub-divide the samples, they were diluted with clean water and fed from an agitated container to a rotary wet sampler capable of dividing the sample into 12 fractions. One stage of sub-division was normally sufficient for samples taken with the probe and three or four stages of sub-division were used for samples of the cyclone products.

The electrolyte for every sample was made up by adding 10 g/lt of $N_a Cl$ and 100 mg/lt of the dispersant Dispex N40. The

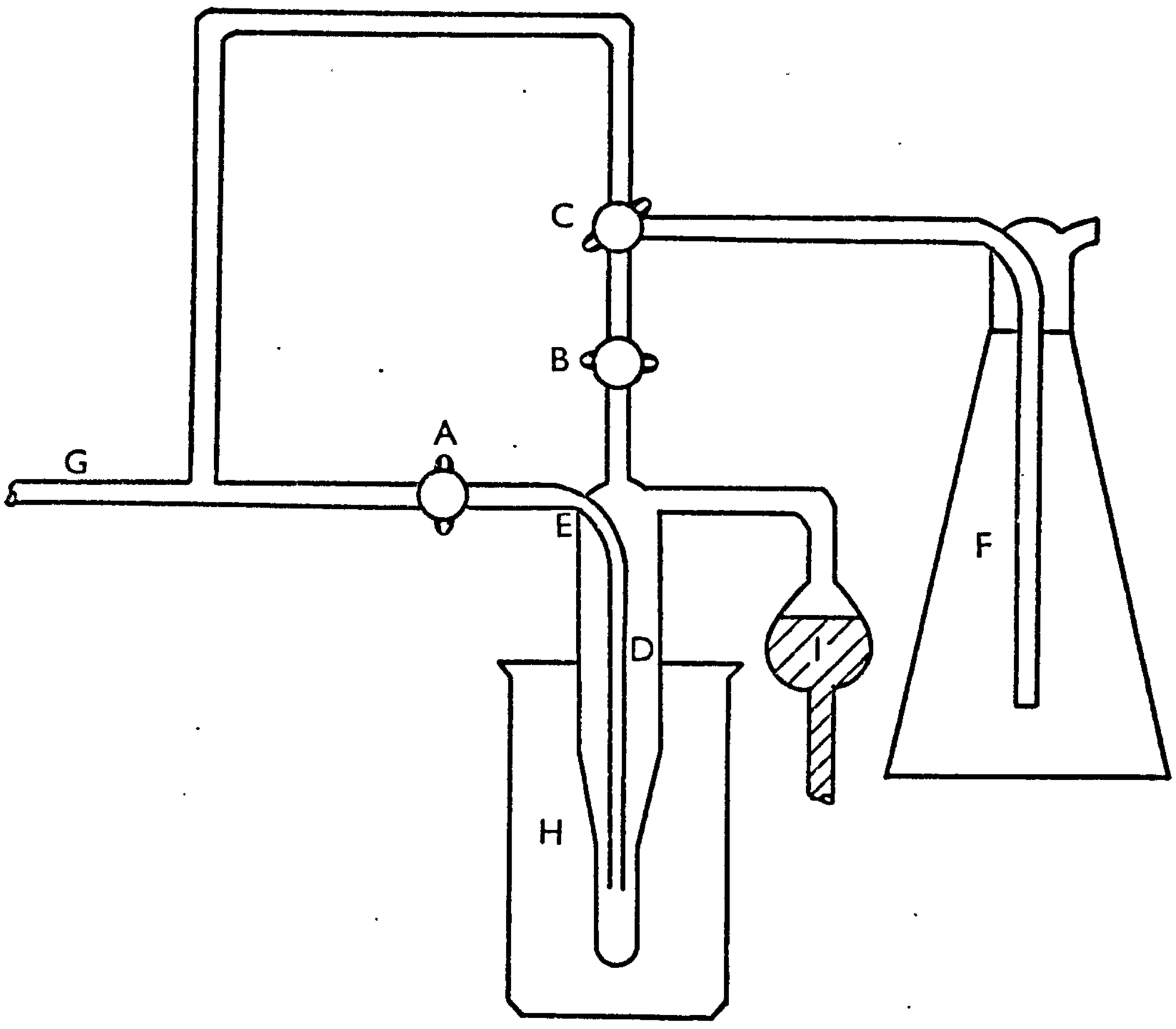

Fig. 25. Sketch of the arrangement to flush away settled particles from the orifice tube.

A, B two-way stopcocks:
C three-way stopcock:
D orifice tube:
E auxiliary outlet:
F clean electrolyte recervoir:
G vacuum line:
H sample:
I mercury manometer.

salt and the dispersant came from concentrated solutions that had been previously passed through 0.45 μm filter papers.

The consumption of sample in every count in the Coulter counter was high, particularly with the 400 μm tube, so, to obtain a sufficient number of counts, at least two sample beakers from the same stage of sub-division were used in every analysis. This also showed that sub-division with the rotary sampler was good.

All other operations including the reduction of data were carried out following the procedures recommended by Coulter Electronics Limited.

APPENDIX 4

TABLES OF DATA

A4.1. Coordinates of the Sampling Positions

The cylindrical coordinates r and z of the sampling positions as defined in art. (2.1) are:

Position	r(mm)	z(mm)
A1	65	370
A2	55	370
A3	45	370
A4	36	370
B1	65	345
B2	55	345
B3	45	345
B4	36	345
B5	33	345
C1	65	319
C2	55	319
C3	45	319
C4	36	319
C5	29	319
D1	70	288
D2	65	288

Position	r(mm)	z(mm)
D3	50	288
D4	35	288
D5	20	288
D6	15	288
D7	9	288
E1	55	226
E2	51	227
E3	41	230
E4	31	232
E5	22	235
E6	12	237
E7	7	239
F1	35	149
F2	30	150
F3	20	152
F4	11	155

The azimuthal coordinate θ for all positions is 60 measured from the cyclone entry in the direction of the feed flow.

A4.2. Data of Tests

Layout of the Tables

(1)	Size	%
(2)	(10)	(11)
(3)		
(4)		
(5)		
(6)		
(7)		
(8)		
(9)		

(1) Sampling position and number of test in that position.

(2) Sampling time, ms.

(3) Solids in feed, weight %.

(4) Solids in underflow, weight %.

(5) Solids in overflow, weight %.

(6) Slurry to underflow, volume %.

(7) Solids to underflow, weight %.

(8) Sampling pressure, atm.

(9) Temperature of slurry, °C.

(10) Particle size at the measured levels, μm.

(11) Cumulative undersize distribution, weight %.

Note: Dashes indicate cases where no data was obtained.

A1.1	Size	%
11.28	6.9	0.3
-	8.7	0.5
-	13.8	1.5
-	22.0	4.5
17.6	34.9	13.1
-	43.9	23.9
1.00	55.3	42.5
25	63.3	58.3
	69.7	67.4
	79.8	82.7
	87.8	88.7
	94.6	94.1
	100.6	95.1
	105.9	97.2
	110.1	97.7
	126.7	98.5
	139.4	98.9

A2.1	Size	%
10.37	6.9	0.3
-	8.7	0.5
-	13.8	1.9
-	22.0	5.3
17.9	34.9	15.1
-	43.9	25.9
1.00	55.3	45.1
25	63.3	61.1
	69.7	71.9
	75.1	79.3
	79.8	83.5
	84.0	90.0
	87.8	91.7
	94.6	94.8
	100.6	96.9
	110.1	98.6
	126.7	98.9

A3.1	Size	%
12.65	6.9	0.3
-	8.7	0.5
-	13.8	1.3
-	22.0	3.6
17.0	34.9	12.8
-	43.9	23.9
1.00	55.3	46.7
25	63.3	62.7
	69.7	73.1
	75.1	82.4
	79.8	85.5
	87.8	91.3
	91.4	94.6
	94.6	95.9
	100.6	97.3
	119.2	99.0
	133.4	99.9

A4.1	Size	%
9.39	6.9	0.8
-	8.7	1.5
-	13.8	3.4
-	22.0	7.9
18.3	34.9	19.1
-	43.9	28.7
1.00	55.3	50.5
25	63.3	64.4
	69.7	74.7
	75.1	81.2
	79.8	88.1
	84.0	89.5
	87.8	93.3
	94.6	96.2
	100.6	98.1
	105.9	98.6
	110.1	99.4

B1.1	Size	%
9.48	6.9	0.3
22.7	8.7	0.5
60.7	13.8	1.7
14.4	22.0	5.1
17.8	34.9	14.7
47.7	43.9	24.5
1.00	55.3	44.1
24	63.3	58.7
	69.7	67.1
	79.8	81.7
	84.0	86.3
	87.8	89.7
	94.6	91.6
	100.6	95.7
	105.9	97.3
	126.7	98.3

B2.1	Size	%
8.64	6.9	0.3
22.3	8.7	0.5
60.4	13.8	1.5
14.3	22.0	4.9
17.1	34.9	13.5
46.6	43.9	23.5
1.00	55.3	41.5
24	63.3	57.3
	69.7	69.1
	75.1	76.8
	79.8	84.6
	84.0	89.5
	87.8	92.2
	94.6	96.3
	100.6	98.1
	110.1	98.9
	126.7	99.8

B3.1	Size	%
9.00	6.9	0.3
22.8	8.7	0.4
60.2	13.8	1.5
14.4	22.0	3.7
16.1	34.9	12.8
48.7	43.9	25.7
1.00	55.3	51.3
25	63.3	68.7
	66.7	75.1
	69.7	80.4
	75.1	88.1
	79.8	92.3
	84.0	95.3
	87.8	97.1
	94.6	98.3
	100.6	99.1
	105.9	99.7

B4.1	Size	%
10.43	6.9	0.1
20.9	8.7	0.3
59.7	13.8	1.2
13.2	22.0	3.2
16.5	34.9	16.9
47.0	43.9	36.3
1.00	50.3	51.7
24	55.3	63.3
	59.6	72.5
	63.3	79.1
	66.7	82.5
	69.7	86.7
	75.1	91.3
	79.8	94.4
	84.0	97.1
	87.8	98.5
	94.6	99.2
	100.6	99.6

B5.1	Size	%
8.42	6.9	0.1
22.7	8.7	0.3
59.9	13.8	1.4
14.5	22.0	4.3
18.1	34.9	18.4
47.9	43.9	37.5
1.00	50.3	54.1
26	55.3	64.3
	63.3	79.1
	66.7	82.7
	69.7	87.7
	75.1	92.7
	79.8	94.9
	84.0	96.5
	87.8	98.0
	94.6	99.2
	100.6	99.4

C1.1	Size	%
8.13	7.0	0.3
21.9	8.8	0.7
60.4	13.9	1.8
13.8	22.1	5.3
17.3	35.1	15.5
47.7	44.2	24.7
1.00	55.7	45.1
24	63.7	58.4
	70.1	69.3
	75.6	78.0
	80.3	82.2
	84.5	88.1
	88.4	90.5
	95.2	94.9
	101.2	97.2
	111.4	98.5
	127.5	100.0

C2.1	Size	%
8.59	7.0	0.2
20.9	8.8	0.4
60.1	13.9	1.5
13.6	22.1	4.7
15.6	35.1	13.6
44.9	44.2	22.9
1.00	55.7	43.3
24	63.7	61.0
	70.1	70.7
	75.6	80.9
	80.3	88.3
	84.5	92.9
	88.4	94.7
	91.9	96.8
	95.2	98.3
	101.2	99.4
	106.5	99.7

C3.1	Size	%
11.77	7.0	0.1
21.7	8.8	0.2
60.0	13.9	1.1
13.9	22.1	3.4
16.9	35.1	12.9
46.7	44.2	27.1
1.00	55.7	50.7
24	63.7	69.9
	70.1	81.3
	75.6	89.9
	80.3	94.3
	84.5	97.3
	88.4	98.3
	91.9	99.1
	95.2	99.7
	101.2	99.9

C4.1	Size	%
9.99	7.0	0.1
20.3	8.8	0.2
60.3	13.9	1.0
12.6	22.1	2.9
16.0	35.1	12.1
47.7	44.2	23.2
1.00	55.7	47.5
24	63.7	68.3
	70.1	83.3
	75.6	92.3
	78.0	95.1
	80.3	96.3
	82.5	98.0
	84.5	98.6
	88.4	99.3
	95.2	99.9
	101.2	100.0

C5.1	Size	%
10.92	6.9	0.1
-	8.7	0.3
-	13.8	0.9
-	22.0	3.1
17.4	34.9	15.7
-	43.9	38.1
1.00	50.3	55.9
25	55.3	70.8
	59.6	80.3
	63.3	86.5
	66.7	91.7
	69.7	94.7
	75.1	97.3
	79.8	98.1
	84.0	99.4
	87.8	99.5
	94.6	99.8

D1.1	Size	%
13.63	6.9	0.1
18.2	8.7	0.2
-	13.8	1.1
11.1	31.6	10.9
18.6	50.2	30.9
50.3	63.2	49.8
1.00	69.5	62.4
28	79.6	80.3
	87.6	89.1
	94.4	93.7
	100.3	96.1
	110.4	97.7
	126.4	98.9
	159.2	99.1

D1.2	Size	%
25.72	6.9	0.1
21.5	8.6	0.2
59.3	13.7	0.8
13.2	31.4	8.5
18.0	49.8	28.2
49.6	62.8	51.1
1.00	69.1	61.7
26	79.1	78.9
	87.1	88.1
	93.8	93.1
	99.7	95.3
	104.9	97.6
	118.2	97.8
	125.6	98.9
	138.2	99.0
	148.9	99.3

D1.3	Size	%
27.27	6.9	0.0
20.8	8.6	0.1
59.0	13.7	0.5
12.9	31.4	5.4
17.3	49.8	23.3
48.9	62.8	45.7
0.38	69.1	58.1
24	79.1	76.5
	83.3	83.3
	87.1	87.7
	93.8	93.6
	99.7	96.2
	104.9	97.1
	118.2	98.1
	125.6	98.2
	138.2	99.0
	148.9	99.6

D2.1	Size	%
12.62	6.9	0.1
22.2	8.7	0.3
59.4	13.8	1.3
12.9	21.9	3.3
19.9	34.8	11.4
53.2	43.8	19.5
1.00	55.2	35.8
28	63.2	48.7
	69.5	62.0
	79.6	76.6
	87.6	88.9
	94.4	92.0
	100.3	96.3
	105.6	96.8
	110.4	97.6
	118.9	98.4
	133.0	99.5

D2.2	Size	%
22.46	7.9	0.6
20.9	10.0	1.1
59.3	31.7	15.0
11.6	50.2	32.5
19.4	63.3	52.5
55.1	72.5	69.0
1.00	79.8	79.3
25	85.9	86.7
	91.3	92.3
	96.1	94.5
	100.5	96.5
	108.2	98.0
	115.0	98.8
	121.1	99.7

D2.3	Size	%
-	7.9	0.7
21.4	10.0	1.3
59.1	19.9	4.1
12.4	31.7	10.2
19.3	50.2	29.6
53.3	63.3	50.7
0.38	72.5	66.0
-	79.8	82.2
	85.9	84.7
	91.3	94.6
	100.5	96.1
	108.2	97.9
	115.0	99.6

D3.1	Size	%
16.70	6.9	0.2
21.4	8.7	0.3
59.0	15.8	1.7
12.9	25.1	5.1
18.5	39.8	14.7
50.8	50.2	28.1
1.00	55.2	32.2
27	63.2	46.5
	69.5	63.2
	74.9	68.6
	79.6	82.7
	83.8	90.1
	87.6	93.3
	91.1	95.9
	94.4	98.8
	100.3	99.6
	105.6	99.9

D3.2	Size	%
26.53	7.9	0.5
19.7	10.0	0.9
59.1	31.7	9.3
11.8	50.2	26.3
16.8	63.3	44.5
50.3	72.5	63.7
1.00	79.8	81.5
24	85.9	90.8
	91.3	95.4
	100.5	98.6
	108.2	99.4
	115.0	99.6

D3.3	Size	%
27.23	7.9	0.5
21.6	10.0	0.9
59.4	31.7	11.0
12.4	50.2	27.3
19.7	63.3	45.6
53.9	72.5	65.3
0.38	79.8	82.3
24	85.9	91.4
	91.3	96.7
	96.1	98.3
	100.5	99.0
	108.2	99.9

D4.1	Size	%
10.48	6.9	0.1
22.0	8.7	0.1
59.6	13.8	0.6
12.8	21.9	2.5
19.7	34.8	7.9
53.3	43.8	14.7
1.00	55.2	27.1
29	63.2	43.2
	69.5	58.8
	74.9	73.4
	79.6	82.9
	83.8	90.8
	87.6	94.6
	91.1	96.7
	94.4	98.7
	100.3	99.5
	105.6	99.9

D4.2	Size	%
13.64	6.9	0.1
20.0	8.7	0.1
59.4	13.8	0.5
11.5	21.9	1.9
17.8	34.8	6.6
52.8	43.8	12.9
1.00	55.2	26.7
29	63.2	42.1
	69.5	58.0
	74.9	73.1
	79.6	84.5
	83.8	91.3
	87.6	95.9
	91.1	97.3
	94.4	98.9
	100.3	99.7
	105.6	99.9

D4.3	Size	%
15.8	6.9	0.1
21.9	8.7	0.1
59.0	13.8	0.5
13.1	21.9	1.9
19.1	34.8	6.7
51.5	43.8	13.3
1.00	55.2	26.2
28	69.5	56.6
	74.9	69.4
	79.6	80.2
	83.8	89.5
	87.6	94.5
	91.1	96.5
	94.4	98.3
	97.4	99.3
	100.3	99.5
	105.6	99.8

D4.4	Size	%
20.83	6.9	0.2
21.7	8.7	0.3
59.5	13.8	1.0
12.9	21.9	2.7
18.9	34.8	8.4
51.9	43.8	13.2
1.00	55.2	37.8
29	63.2	40.9
	69.5	59.6
	74.9	72.9
	79.6	83.3
	83.8	90.3
	87.6	94.8
	91.1	98.0
	94.4	98.6
	100.3	99.5
	105.6	99.9

D4.5	Size	%
28.78	7.9	0.5
21.0	10.0	1.0
60.7	31.7	10.4
11.8	36.2	12.8
18.9	50.2	24.4
54.7	63.3	43.6
1.00	72.5	65.2
28	79.8	81.6
	85.9	90.6
	91.3	96.0
	96.1	98.8
	100.5	99.5

D4.6	Size	%
-	7.9	0.6
20.6	10.0	1.0
59.5	31.7	11.6
11.9	50.2	24.9
18.3	68.2	57.3
52.9	76.3	77.3
0.39	79.8	81.5
29	85.9	92.7
	91.3	97.2
	96.1	90.0
	100.5	99.9

D4.7	Size	%
55.73	6.9	0.1
22.4	8.7	0.2
59.8	13.8	0.6
14.0	21.9	2.1
18.4	34.8	7.6
49.2	43.8	14.5
1.00	55.2	27.2
29	63.2	42.5
	69.5	57.3
	74.9	70.7
	79.6	82.2
	83.8	88.4
	87.6	92.8
	91.1	96.2
	94.4	98.2
	97.4	99.2
	100.3	99.6
	105.6	99.8

D5.1	Size	%
10.39	6.9	0.0
22.3	8.7	0.1
58.4	13.8	0.5
13.7	21.9	1.9
19.2	34.8	6.1
50.3	43.8	11.7
1.00	55.2	25.1
28	63.2	39.6
	69.5	54.2
	74.9	71.2
	79.6	81.9
	83.8	90.3
	87.6	95.2
	91.1	97.6
	94.4	98.7
	97.4	99.5
	100.3	99.7
	105.6	99.9

D5.2	Size	%
59.56	7.9	0.5
21.1	10.0	1.0
58.7	19.9	3.0
12.5	50.2	26.7
18.5	63.3	50.7
51.5	72.5	70.3
1.00	76.3	79.4
24	79.8	87.0
	85.9	93.9
	91.3	97.9
	100.5	99.7

D5.3	Size	%
60.22	7.9	0.5
19.2	10.0	0.9
60.2	31.7	10.8
11.2	57.5	32.4
16.3	63.3	48.5
51.1	72.5	71.3
0.38	76.3	80.5
24	79.8	87.5
	85.9	95.1
	91.3	98.1
	96.1	99.6
	100.5	99.7

D6.1	Size	%
11.45	6.9	0.0
21.6	8.7	0.1
58.4	13.8	0.5
12.8	21.9	1.6
19.2	34.8	6.0
52.0	43.8	12.8
1.00	55.2	33.9
27	63.2	55.0
	69.5	74.2
	74.9	86.2
	79.6	93.4
	83.8	96.9
	87.6	98.2
	91.1	99.4
	94.4	99.7
	97.4	99.9

D6.2	Size	%
14.78	6.9	0.1
21.2	8.6	0.2
59.7	21.8	3.1
13.1	34.6	7.3
17.4	49.8	20.5
49.0	54.9	30.6
1.00	62.8	47.8
24	66.1	60.5
	69.1	68.9
	74.5	84.7
	79.1	90.8
	83.3	96.0
	87.1	98.3
	93.8	99.6

D6.3	Size	%
15.32	6.9	0.0
21.6	8.6	0.1
59.5	21.8	2.1
13.3	34.6	5.1
17.8	49.8	20.3
49.2	54.9	29.6
0.38	62.8	46.6
25	66.1	57.3
	69.1	65.4
	74.5	79.9
	79.1	89.1
	83.3	94.2
	87.1	96.5
	93.8	98.9
	99.7	99.9

D7.1	Size	%
9.79	6.9	0.1
21.9	8.7	0.3
59.5	13.8	0.7
12.9	21.9	2.7
19.5	34.8	16.5
52.7	43.8	36.1
1.00	50.2	48.9
29	55.2	61.1
	59.5	70.1
	63.2	77.1
	66.5	83.1
	69.5	86.9
	74.9	91.5
	79.6	96.9
	83.8	98.7
	87.6	99.4
	94.4	99.9

D7.2	Size	%
10.63	6.9	0.1
22.6	8.7	0.3
59.0	13.8	1.2
13.5	21.9	4.3
20.0	34.8	19.1
52.1	43.8	37.2
1.00	50.2	54.4
29	55.2	66.9
	59.5	76.1
	63.2	82.7
	66.5	87.9
	69.5	90.7
	74.9	95.2
	79.6	97.9
	83.8	98.7
	87.6	99.3
	94.4	99.8

D7.3	Size	%
11.41	6.9	0.1
20.4	8.7	0.2
59.8	13.8	1.0
11.9	21.9	3.2
17.7	34.8	13.0
51.9	43.8	31.9
1.00	50.2	49.0
30	55.2	64.1
	59.5	74.0
	63.2	82.8
	66.5	87.9
	69.5	91.7
	74.9	96.5
	79.6	98.1
	83.8	99.5
	87.6	99.6
	94.4	99.9

D7.4	Size	%
14.04	6.9	0.1
22.0	8.7	0.2
59.5	13.8	1.2
13.4	21.9	4.3
18.6	34.8	17.7
50.4	43.8	33.6
1.00	50.2	45.5
28	55.2	55.5
	59.5	67.8
	63.2	76.3
	66.5	80.5
	69.5	85.5
	74.9	92.9
	79.6	96.3
	83.8	98.1
	87.6	98.9
	94.4	99.5

D7.5	Size	%
20.62	6.9	0.2
22.4	8.7	0.3
59.9	13.8	1.1
13.0	21.9	3.5
20.1	34.8	11.2
53.6	43.8	20.5
1.00	50.2	27.3
30	55.2	38.5
	59.5	45.5
	63.2	57.0
	66.5	63.1
	69.5	70.7
	74.9	83.4
	79.6	89.7
	83.8	96.0
	87.6	98.2
	94.4	99.6

D7.6	Size	%
34.65	6.9	0.1
-	8.7	0.3
-	13.8	1.1
-	21.9	3.4
-	34.8	10.4
-	43.8	17.2
1.00	50.2	25.9
30	55.2	33.2
	59.5	43.1
	63.2	50.0
	66.5	58.7
	69.5	66.9
	74.9	81.7
	79.6	87.8
	83.8	93.2
	87.6	97.8
	94.4	99.2
	100.3	99.9

E1.1	Size	%
14.43	6.9	0.1
21.7	8.7	0.1
58.6	13.8	0.5
13.8	21.9	2.1
17.5	34.8	9.1
47.3	50.2	25.5
1.00	63.3	46.3
25	75.0	65.3
	83.9	81.1
	87.7	84.8
	94.5	91.5
	100.4	94.1
	110.5	95.6
	126.5	97.7
	139.3	98.7
	159.4	98.9

E1.2	Size	%
-	6.9	0.1
22.3	8.7	0.2
62.3	13.7	0.9
13.5	21.8	2.9
18.0	34.6	9.5
50.4	50.0	24.5
1.00	63.0	45.8
27	74.6	67.6
	79.3	72.6
	83.5	80.9
	87.3	86.3
	94.0	92.7
	99.9	94.4
	110.0	97.5
	125.9	98.6
	138.6	99.6

E1.3	Size	%
19.79	6.9	0.1
22.2	8.7	0.2
58.7	13.7	0.7
12.8	21.8	0.9
20.4	34.6	7.5
54.1	50.0	23.8
0.38	63.0	44.2
30	74.6	66.6
	79.3	74.7
	83.5	82.9
	87.3	86.0
	94.0	93.2
	99.9	94.6
	110.0	97.4
	138.6	98.6
	158.6	99.8

E2.1	Size	%
12.96	6.9	0.1
21.9	8.7	0.1
59.8	13.8	0.7
13.5	21.9	2.9
18.2	34.8	10.8
49.7	50.2	25.1
1.00	63.3	48.1
25	69.6	56.7
	79.7	76.3
	83.9	81.7
	87.7	85.8
	94.5	92.2
	100.4	94.0
	105.7	96.2
	110.5	97.4
	119.1	97.9
	133.2	98.7
	150.0	99.3

E2.2	Size	%
25.54	6.9	0.1
19.1	8.7	0.2
59.3	13.8	0.7
10.4	21.9	3.3
17.9	34.8	9.6
55.5	50.2	24.6
0.38	63.2	46.2
28	74.9	69.2
	83.8	84.4
	87.6	88.7
	94.4	93.4
	100.3	96.5
	105.6	98.2
	118.9	98.6
	133.0	99.1
	139.1	99.7

E2.3	Size	%
26.07	6.9	0.1
22.3	8.7	0.2
60.1	13.9	0.7
13.2	22.0	2.9
19.4	34.9	9.1
52.2	50.4	24.1
1.00	63.5	45.5
28	69.9	57.4
	80.0	71.9
	84.2	79.0
	88.1	84.6
	94.9	91.4
	100.8	94.5
	106.1	96.4
	110.9	97.1
	119.5	98.3
	133.7	99.0

E3.1	Size	%
14.00	6.9	0.1
21.4	8.7	0.1
59.0	13.8	0.7
12.8	21.9	2.4
18.6	34.8	7.9
51.3	50.2	21.9
1.00	63.3	38.3
25	69.6	51.3
	79.7	72.7
	83.9	79.1
	87.7	85.1
	91.2	89.3
	94.5	92.7
	97.6	94.9
	100.4	96.7
	105.7	98.7
	110.5	98.9
	126.5	99.7

E3.2	Size	%
14.80	6.9	0.1
23.7	8.7	0.2
59.4	13.9	0.7
14.6	22.0	2.4
20.3	34.9	7.6
50.9	50.4	21.6
0.38	63.5	41.2
28	69.9	53.4
	80.0	71.3
	84.2	79.4
	88.1	86.6
	94.9	93.3
	100.8	96.4
	106.1	98.8
	110.9	99.2
	119.5	99.4
	127.0	100.0

E3.3	Size	%
18.84	6.9	0.1
21.3	8.7	0.2
59.3	13.9	1.0
13.0	22.0	3.0
18.0	34.9	8.8
50.0	50.4	22.5
1.00	63.5	40.6
28	69.9	52.5
	80.0	72.7
	84.2	81.8
	88.1	86.5
	94.9	92.3
	100.8	96.4
	106.1	98.6
	110.9	99.9
	119.5	100.0

E4.1	Size	%
12.20	6.9	0.0
21.7	8.7	0.1
58.7	13.8	0.3
13.3	21.9	1.5
18.5	34.8	7.0
50.2	50.2	16.6
1.00	63.3	38.6
25	75.0	60.8
	79.7	69.9
	83.9	79.2
	87.7	85.1
	94.5	92.9
	97.6	94.7
	100.4	97.0
	103.1	98.0
	105.7	98.7
	110.5	99.4
	119.1	99.7

E4.2	Size	%
-	8.7	0.0
21.9	13.9	0.1
59.3	22.0	0.9
12.8	34.9	4.6
19.5	50.4	15.6
53.0	63.5	35.8
0.38	69.9	46.6
27	80.0	70.6
	84.2	79.2
	88.1	86.4
	94.9	93.9
	100.8	97.6
	106.1	99.1
	110.9	99.5
	119.5	99.9

E4.3	Size	%
20.65	6.9	0.1
19.5	8.7	0.2
59.9	13.9	0.7
10.9	22.0	2.1
17.6	34.9	6.3
54.0	50.4	19.0
0.38	63.5	39.0
28	69.9	51.9
	80.0	75.8
	84.2	85.2
	88.1	88.9
	94.9	96.2
	100.8	98.3
	106.1	99.3
	110.9	99.9
	119.5	100.0

E4.4	Size	%
47.58	6.9	0.1
21.3	8.7	0.1
59.9	13.9	0.6
13.0	22.0	1.8
17.8	34.9	6.2
49.9	50.4	17.3
0.38	63.5	37.4
27	69.9	48.0
	80.0	68.0
	84.2	76.9
	88.1	85.6
	94.9	92.3
	100.8	96.7
	106.1	98.4
	110.9	99.3
	119.5	99.5

E4.5	Size	%
-	6.9	0.0
22.3	8.7	0.0
59.6	13.9	0.5
13.8	22.0	1.7
18.5	34.9	6.2
49.5	50.4	18.6
1.00	63.5	38.2
27	69.9	49.3
	80.0	69.9
	84.2	78.0
	88.1	84.3
	94.9	92.4
	100.8	96.7
	106.1	98.6
	110.9	99.3
	119.5	99.9

E5.1	Size	%
11.92	7.0	0.1
21.9	8.8	0.1
58.9	14.0	0.7
13.1	22.1	2.1
19.3	35.2	6.4
51.8	50.7	16.1
1.00	63.9	36.5
27	70.3	45.4
	80.5	66.9
	84.7	78.1
	88.6	83.3
	92.1	89.6
	95.4	91.3
	98.5	94.7
	101.4	96.9
	106.8	98.1
	111.6	99.3
	120.2	99.9

E5.2	Size	%
20.79	7.0	0.1
22.6	8.8	0.2
58.8	14.0	0.7
14.0	22.1	1.9
19.1	35.2	5.8
49.7	50.7	14.8
1.00	63.9	33.7
26	70.3	45.0
	80.5	66.3
	84.7	73.9
	88.6	82.4
	92.1	88.5
	95.4	92.5
	101.4	96.0
	106.8	98.6
	111.6	99.2
	120.2	99.9

E5.3	Size	%
35.32	7.0	0.1
21.9	8.8	0.1
61.4	13.9	0.5
12.3	22.1	1.6
19.6	35.0	6.6
55.0	50.5	18.5
1.00	63.7	38.0
27	70.1	49.7
	80.2	71.5
	84.4	79.2
	88.3	86.0
	91.8	90.3
	95.1	92.9
	101.0	97.2
	106.4	98.9
	111.2	99.4
	119.8	99.7

E5.4	Size	%
-	6.9	0.1
22.3	8.7	0.2
59.3	13.9	0.7
14.0	22.0	2.3
18.4	34.9	6.3
48.9	50.4	19.2
1.00	63.5	39.6
27	69.9	51.2
	80.0	70.2
	84.2	79.0
	88.1	86.7
	94.9	95.0
	100.8	97.3
	106.1	98.6
	110.9	99.3
	119.5	99.8

E5.5	Size	%
58.16	6.9	0.0
22.1	8.7	0.1
59.4	13.9	0.5
13.4	22.0	1.4
19.0	34.9	7.3
51.0	50.4	20.9
0.38	63.5	41.3
27	69.9	52.2
	80.0	74.0
	84.2	81.5
	88.1	87.0
	94.9	94.5
	100.8	97.4
	106.1	99.1
	110.9	99.5
	119.5	99.8

E5.6	Size	%
132.60	7.0	0.1
22.0	8.8	0.1
58.5	13.9	0.6
13.8	22.1	2.0
18.5	35.0	6.9
49.0	50.5	19.1
1.00	63.7	39.4
26	70.1	48.8
	80.2	70.7
	88.3	84.1
	91.8	89.3
	95.1	91.5
	101.0	96.0
	106.4	98.2
	111.2	98.9
	119.8	99.5
	127.3	99.7

E5.7	Size	%
4812.00	7.0	0.2
-	8.8	0.3
-	13.9	1.0
-	22.1	3.2
-	35.0	11.3
-	50.5	31.0
1.00	55.6	40.1
25	63.7	55.1
	70.1	64.9
	80.2	82.3
	84.4	86.7
	88.3	90.9
	91.8	93.5
	95.1	94.7
	98.2	97.2
	101.0	97.3
	111.2	98.7
	127.3	99.0

E6.1	Size	%
10.65	7.0	0.1
22.3	8.8	0.1
58.5	14.0	0.7
13.7	22.1	1.9
19.1	35.2	6.3
50.2	50.7	19.8
1.00	63.9	43.6
26	70.3	57.3
	75.8	70.2
	80.5	80.5
	84.7	86.7
	88.6	92.3
	92.1	95.2
	95.4	97.0
	98.5	98.6
	101.4	98.9
	106.8	99.7
	111.6	99.7

E6.2	Size	%
32.07	6.9	0.1
21.1	8.7	0.2
58.7	13.9	0.9
13.2	22.0	2.8
17.5	34.9	9.5
48.7	50.4	23.8
0.38	55.5	32.0
26	63.5	45.3
	69.9	55.6
	75.3	65.9
	80.0	77.5
	84.2	84.0
	88.1	89.6
	94.9	95.4
	100.8	98.6
	106.1	99.3
	110.9	99.8

E6.3	Size	%
37.80	6.9	0.1
21.9	8.7	0.2
59.8	13.9	1.0
13.8	22.0	2.2
17.6	34.9	9.6
48.0	50.4	22.9
1.00	63.5	42.7
26	69.9	53.3
	75.3	63.4
	80.0	73.1
	84.2	81.4
	88.1	86.4
	94.9	93.8
	100.8	98.0
	106.1	98.2
	110.9	99.2
	119.5	100.0

E7.1	Size	%
11.85	7.0	0.1
22.1	8.8	0.3
58.9	14.0	0.9
13.5	22.1	3.1
19.0	35.2	13.3
50.5	44.3	28.7
1.00	50.7	43.3
27	55.8	54.0
	63.9	73.3
	70.3	83.9
	75.8	90.2
	80.5	93.7
	84.7	96.6
	88.6	98.4
	92.1	98.6
	95.4	99.3
	98.5	99.7
	101.4	99.9

E7.2	Size	%
26.71	6.9	0.1
22.1	8.7	0.3
60.0	13.9	1.1
13.3	22.0	3.0
18.9	34.9	9.3
51.4	50.4	24.8
1.00	63.5	43.2
27	69.9	56.7
	75.3	68.1
	80.0	76.0
	84.2	82.4
	88.1	89.2
	94.9	96.6
	100.8	97.3
	106.1	99.2

E7.3	Size	%
36.77	6.9	0.1
22.5	8.7	0.2
59.8	13.9	0.9
13.5	22.0	2.2
19.3	34.9	7.2
51.3	50.4	19.8
0.38	63.5	39.2
27	69.9	50.8
	75.3	63.6
	80.0	74.0
	84.2	80.1
	88.1	88.0
	94.9	94.5
	100.8	97.2
	106.1	99.3
	110.9	99.5

F1.1	Size	%
13.27	6.9	0.1
21.8	8.7	0.1
58.3	13.8	0.5
13.3	21.9	1.9
18.7	34.8	7.5
50.3	50.2	21.9
1.00	63.3	39.5
26	69.6	49.9
	79.7	66.1
	87.7	80.9
	94.5	86.6
	100.4	90.9
	105.7	93.9
	110.5	95.9
	126.5	97.2
	139.3	98.5
	159.4	99.1

F1.2	Size	%
23.41	6.9	0.1
21.7	8.7	0.2
58.9	13.9	0.6
13.8	22.0	1.9
17.6	44.0	13.1
47.7	55.4	23.9
1.00	69.8	45.8
26	79.9	65.5
	87.9	79.2
94.7	86.8	
100.7	91.1	
106.0	94.1	
110.8	96.1	
139.6	98.0	
159.8	99.5	

F1.3	Size	%
30.37	6.9	0.0
21.3	8.7	0.1
56.7	22.0	2.6
13.8	34.9	8.3
17.5	55.4	26.1
46.6	69.8	49.9
0.38	79.9	67.9
25	87.9	80.1
	94.7	87.3
100.7	91.1	
106.0	93.8	
110.8	95.4	
126.8	98.0	
139.6	98.5	
159.8	99.4	

F2.1	Size	%
11.81	6.9	0.1
20.8	8.7	0.1
58.7	13.8	0.7
12.2	21.9	2.3
18.4	34.8	8.0
52.0	50.2	20.5
1.00	63.3	38.2
26	69.6	50.7
	79.7	66.7
	87.7	78.3
	94.5	87.7
	100.4	91.6
	105.7	94.9
	110.5	95.7
	126.5	98.1
	139.3	98.7

F2.2	Size	%
37.56	6.9	0.0
21.9	8.7	0.1
59.5	22.0	2.1
13.7	34.9	6.3
17.7	55.4	25.9
48.3	69.8	46.9
0.38	79.9	64.4
24	87.9	78.9
	94.7	87.0
	100.7	91.6
	106.0	94.4
	110.8	95.6
	126.8	97.5
	139.6	98.7
	159.8	99.5

F2.3	Size	%
40.44	6.9	0.1
21.5	8.7	0.1
59.5	22.0	2.1
13.5	44.0	9.3
17.3	55.4	28.9
48.0	69.8	49.8
1.00	79.9	67.8
25	87.9	79.4
	94.7	89.9
	100.7	92.8
	106.0	96.2
	110.8	97.1
	119.4	98.3
	133.5	98.7
	139.6	99.3

F3.1	Size	%
12.88	6.9	0.0
21.2	8.7	0.1
59.2	13.8	0.3
12.7	21.9	1.9
18.3	34.8	7.9
51.1	50.2	20.3
1.00	63.3	37.5
27	69.6	46.9
	79.7	66.6
	87.7	81.2
	94.5	87.5
	100.4	92.1
	105.7	94.5
	110.5	95.4
	126.5	97.5
	139.3	98.8

F3.2	Size	%
35.05	6.9	0.0
20.7	8.7	0.1
58.7	22.0	2.3
12.8	44.0	12.2
17.1	55.4	22.6
48.5	69.8	45.3
1.00	79.9	65.1
24	87.9	77.9
	94.7	87.5
	100.7	93.4
	106.0	95.4
	110.8	96.9
	119.4	98.3
	126.8	99.2
	133.5	99.3

F3.3	Size	%
42.57	6.9	0.0
22.0	8.7	0.1
59.6	13.9	0.4
14.1	22.0	1.4
17.4	44.0	12.4
47.2	55.4	22.4
0.38	69.8	44.1
25	79.9	61.9
	87.9	75.7
	94.7	85.5
	100.7	91.4
	106.0	92.2
	110.8	94.7
	126.8	96.9
	139.6	98.6
	159.8	99.6

F4.1	Size	%
12.7¼	6.9	0.1
20.5	8.7	0.1
58.9	13.8	0.5
12.4	21.9	1.7
17.5	34.8	5.0
50.1	50.2	16.1
1.00	63.3	31.7
26	69.6	44.2
	79.7	65.2
	87.7	79.8
	94.5	89.6
	100.4	93.5
	105.7	96.1
	110.5	97.5
	126.5	98.7
	139.3	99.5

F4.2	Size	%
52.05	7.0	0.1
20.2	8.8	0.1
60.1	22.2	2.8
11.9	35.2	6.8
17.3	56.0	25.8
51.5	70.5	48.1
1.00	80.7	67.6
27	84.9	75.6
	88.8	81.7
	95.7	88.0
	101.7	93.7
	107.0	95.7
	111.9	96.2
	128.1	98.8
	141.0	99.1
	161.4	99.8

F4.3	Size	%
55.91	6.9	0.0
19.7	8.7	0.1
59.4	22.0	2.2
10.1	44.0	14.2
19.4	55.4	28.1
58.5	69.8	55.0
0.38	79.9	74.4
26	87.9	86.2
	94.7	92.5
	100.7	96.7
	106.0	97.1
	110.8	98.5
	119.4	99.1
	126.8	99.3
	133.5	99.6

REFERENCES

1. Bretney, E., U.S. Pat. No. 453, 105 (May, 26, 1891).
2. Bradley, D., The Hydrocyclone, Pergamon Press, (1965).
3. Kelsall, D.F., Trans. Instn. Chem. Engs., 30, 87-108, (1952).
4. Bradley, D. and Pulling, D.J., Trans. Inst. Chem. Engrs., 37, 34-45, (1959).
5. Dahlstrom, D.A., Trans. Amer. Inst. of Min. and Metall. Engrs., 184, 331-344, (1949).
6. Fontein, F.J. and Dijksman, C., Inst. Min. and Met. Symp. on Recent Developments in Mineral Dressing, 229-257, (1952).
7. Bradley, D., Ind. Chemist, 34, 473-480, (1958).
8. Rietema, K., Chem. Eng. Sci., 15, 310-319, (1961).
9. Lapple, C.E. and Shepherd, C.B., Ind. Eng. Chem., 32, 605-617, (1940).
10. Tchen, C.M., "Mean Value and Correlation Problems Connected with the Motion of Small Particles Suspended in a Turbulent Fluid", Ph.D. Thesis, Delft, (1947).
11. Hinze, J.O., "Turbulence", McGraw-Hill, (1959).
12. Soo, S.L., "Fluid Dynamics of Multiphase Systems", Blaisdell, (1967).
13. Cohen, E. et al., Trans. Inst. Min. and Met., 75, C129-138, (1966).
14. Badzioch, S., Brit. J. App. Phys., 10, 26-32, (1959).
15. Coulter Electronics Ltd., Instruction Manual for Coulter Counter Model ZB (Industrial), (Feb., 1975).

ACKNOWLEDGEMENTS

I wish to express my gratitude to Professor E. Cohen for his valuable guidance and encouragement throughout the course of this project.

I am also grateful to Mr. H. Fairbrother for his assistance in the analysis of the solution to the mathematical model.

My thanks are due to the technical staff of the Department of Mining and Mineral Technology for the willing assistance received in the construction of experimental equipment.

I am particularly indebted to the British Government and to the University of Chile for the scholarship that enabled me to carry out this research.